Received: 25 August 2022 | Revised: 19 December 2022 | Accepted: 12 March 2023

DOI: 10.1111/gcb.16709

Global Change Biology WILEY

RESEARCH ARTICLE

Phytoplankton life strategies, phenological shifts and climate change in the North Atlantic Ocean from 1850 to 2100

Loïck Kléparski[1,2] | Grégory Beaugrand[1] | Martin Edwards[3,4] | Clare Ostle[2]

[1]Univ. Littoral Côte d'Opale, CNRS, Univ. Lille, UMR 8187 – LOG – Laboratoire d'Océanologie et de Géosciences, Wimereux, France

[2]Marine Biological Association, Plymouth, UK

[3]Plymouth Marine Laboratory, Plymouth, UK

[4]School of Biological and Marine Sciences, University of Plymouth, Plymouth, UK

Correspondence
Loïck Kléparski, Univ. Littoral Côte d'Opale, CNRS, Univ. Lille, UMR 8187 – LOG – Laboratoire d'Océanologie et de Géosciences, F-62930 Wimereux, France.
Email: loick.kleparski@hotmail.fr

Abstract

Significant phenological shifts induced by climate change are projected within the phytoplankton community. However, projections from current Earth System Models (ESMs) understandably rely on simplified community responses that do not consider evolutionary strategies manifested as various phenotypes and trait groups. Here, we use a species-based modelling approach, combined with large-scale plankton observations, to investigate past, contemporary and future phenological shifts in diatoms (grouped by their morphological traits) and dinoflagellates in three key areas of the North Atlantic Ocean (North Sea, North-East Atlantic and Labrador Sea) from 1850 to 2100. Our study reveals that the three phytoplanktonic groups exhibit coherent and different shifts in phenology and abundance throughout the North Atlantic Ocean. The seasonal duration of large flattened (i.e. oblate) diatoms is predicted to shrink and their abundance to decline, whereas the phenology of slow-sinking elongated (i.e. prolate) diatoms and of dinoflagellates is expected to expand and their abundance to rise, which may alter carbon export in this important sink region. The increase in prolates and dinoflagellates, two groups currently not considered in ESMs, may alleviate the negative influence of global climate change on oblates, which are responsible of massive peaks of biomass and carbon export in spring. We suggest that including prolates and dinoflagellates in models may improve our understanding of the influence of global climate change on the biological carbon cycle in the oceans.

KEYWORDS
annual phytoplankton succession, climate change, diatoms, dinoflagellates, oblates, phenology, prolates

1 | INTRODUCTION

Current Earth System Models (ESMs) are projecting a decline in phytoplankton abundance (Bopp et al., 2013; Dutkiewicz et al., 2013; IPCC, 2019; Kwiatkowski et al., 2020) and anticipate significant phenological shifts (Asch et al., 2019; Henson et al., 2013, 2018; Yamaguchi et al., 2022) that may lead to trophic desynchronisation and community reorganisation (Edwards & Richardson, 2004; IPCC, 2019; Winder & Schindler, 2004; Yamaguchi et al., 2022). Phenological shifts in phytoplankton are expected because of ocean warming (and also freshening in the poles) and its strengthening influence on water column stability, which is expected to diminish nutrients supply in the euphotic zone, favouring small phytoplankton (e.g. nanoplankton and picoplankton) at the expense of diatoms

(Bopp et al., 2005; Marinov et al., 2010), a major group thought to be responsible for 40% of total marine primary production (Field et al., 1998; Tréguer et al., 2018).

Although shifts in phytoplankton phenology are now widely observed among marine and freshwater ecosystems (Friedland et al., 2018; Poloczanska et al., 2013; Thackeray et al., 2016), the examination of diatom seasonality in some regions of the North Atlantic suggests a relative stability (Chivers et al., 2020; Edwards & Richardson, 2004). These unexpected results may originate from the range of strategies that have been developed by diatoms and enable them to occur in diverse environments (Kemp & Villareal, 2013, 2018). Among those strategies, diatom morphological traits might have an important influence on species phenology (Kléparski et al., 2022). Indeed, it has recently been shown that diatom cell shape has evolved as a key adaptation that confers to a species a specific phenology, oblate (i.e. flattened) diatoms being dominant in well-mixed, nutrients-rich, low-stratified waters, whereas prolate (i.e. elongated) diatoms dominate in the stratified low-nutrient waters (Kléparski et al., 2022). Cell elongation of prolate diatoms enhances their buoyancy without altering their capacity to absorb nutrients, conferring them a selective advantage in stratified low-nutrient waters (Kléparski et al., 2022).

Most projected phenological shifts (Asch et al., 2019; Henson et al., 2013, 2018; Yamaguchi et al., 2022), which rely on the analyses of variables such as chlorophyll concentration or net primary production, originate from ESMs that only consider a few phytoplankton types (only one for diatoms and none for dinoflagellates). Therefore, those models cannot anticipate subtle changes in phytoplankton community (Kemp & Villareal, 2018; Séférian et al., 2020; Tréguer et al., 2018) and some discrepancies have been reported between satellite observations and model projections (Cabré et al., 2016). Here we applied a species-based modelling approach, combined with large-scale plankton observations, to investigate past, contemporary and future long-term changes (1850–2100) in the phenology of oblates, prolates and dinoflagellates using six ESMs and two climate warming scenarios (a medium and a high emission scenario, i.e. SSP2-4.5 and SSP5-8.5).

2 | MATERIALS AND METHODS

2.1 | Biological data

Phytoplankton data came from the continuous plankton recorder (CPR) survey. The CPR is a long-term plankton monitoring programme that has collected plankton on a monthly basis in the North Atlantic Ocean and its adjacent seas since 1946. The sampling instrument is a high-speed plankton recorder towed behind voluntary merchant ships (called 'ships of opportunity') at a depth of approximately 7 m (Beaugrand et al., 2003; Reid et al., 2003). As phytoplankton sampling remained unchanged since 1958 (Warner & Hays, 1994) and historical climatic simulations ended in 2014 (see Section 2.2 below), we used the abundance data collected for the diatoms and the dinoflagellates between 1958 and 2014. Each value of abundance corresponds to a number of cells per CPR sample, which corresponds to ~3 m^3 of seawater filtered (Jonas et al., 2004). Species that were first identified after 1958 were discarded from the analyses. To account for the climatic variability that was observed in the North Atlantic sector during the period (Beaugrand et al., 2019; Edwards et al., 2002) and minimise the noise associated with the CPR sampling (e.g. exceptional high abundance caused by local hydro-meteorological events, patchiness or abundance misestimation), we calculated a daily mean abundance climatology (based on 365 days) for each species for three 18-year periods: 1958–1976, 1977–1995 and 1996–2014 (a total of 365 days × 3 = 1095 days). The three periods were chosen to be of even length. Therefore, we were able to consider the seasonal signal and the long-term trend, which would have been impossible by using a single climatology based on the entire available time period (Mannocci et al., 2017). Climatologies were estimated in three distinct oceanic regions of the North Atlantic: (i) the North Sea (51°N to 60°N, −3°E to 9°E), (ii) the North-East Atlantic (61°N to 63.5°N, −21°E to −8°E) and (iii) the Labrador Sea (48°N to 60°N, −55°E to −40°E). Climatologies were calculated in a given region for the species/taxa that were present in more than 100 CPR samples. A total of 44 species/taxa were therefore selected (Table S1). Climatologies (for the three periods) were smoothed in each region by means of a double 6-order simple moving average (i.e. 13-day window) and subsequently standardised between 0 and 1, applying the approach of Caracciolo et al. (2021). Standardisation was performed as follows:

$$A^{*}_{(i,j)} = \frac{A_{ij}}{\max\left(A_j\right)} \quad (1)$$

with $A^{*}_{(i,j)}$ the standardised abundance of species j on day i, A_{ij} the abundance of species j on day i and $\max\left(A_j\right)$ the maximal abundance of species j in the three regions (i.e. North Sea, North-East Atlantic and Labrador Sea) between 1958 and 2014. By doing so, the variations in $A^{*}_{(i,j)}$ reflect both the differences within and between the three regions. We then estimated the 90th percentile of the abundance (P90) of each species using the non-standardised daily climatologies in the three oceanic regions (Table S1).

Species were divided into three groups: oblate and prolate diatoms and dinoflagellates, which are known to have distinct environmental requirements (Irwin et al., 2012; Kléparski et al., 2022; Table S1). The oblate group gathered diatoms (species or taxa) that have a mean cell diameter greater than their mean cell height and the prolate group the diatoms (species or taxa) that have a mean cell diameter smaller than their mean cell height. Information on diatom cell shapes were retrieved from Kléparski et al. (2022; their figure 3). Mean monthly abundances between 1958 and 2014 were estimated for each group and in each oceanic region (Figure 1a–i). Data were subsequently smoothed by means of a first-order simple moving average (i.e. 3-month smoothing window) and then standardised between 0 and 1 using the 90th percentile of the monthly abundance of each taxonomic group ($P90_m$):

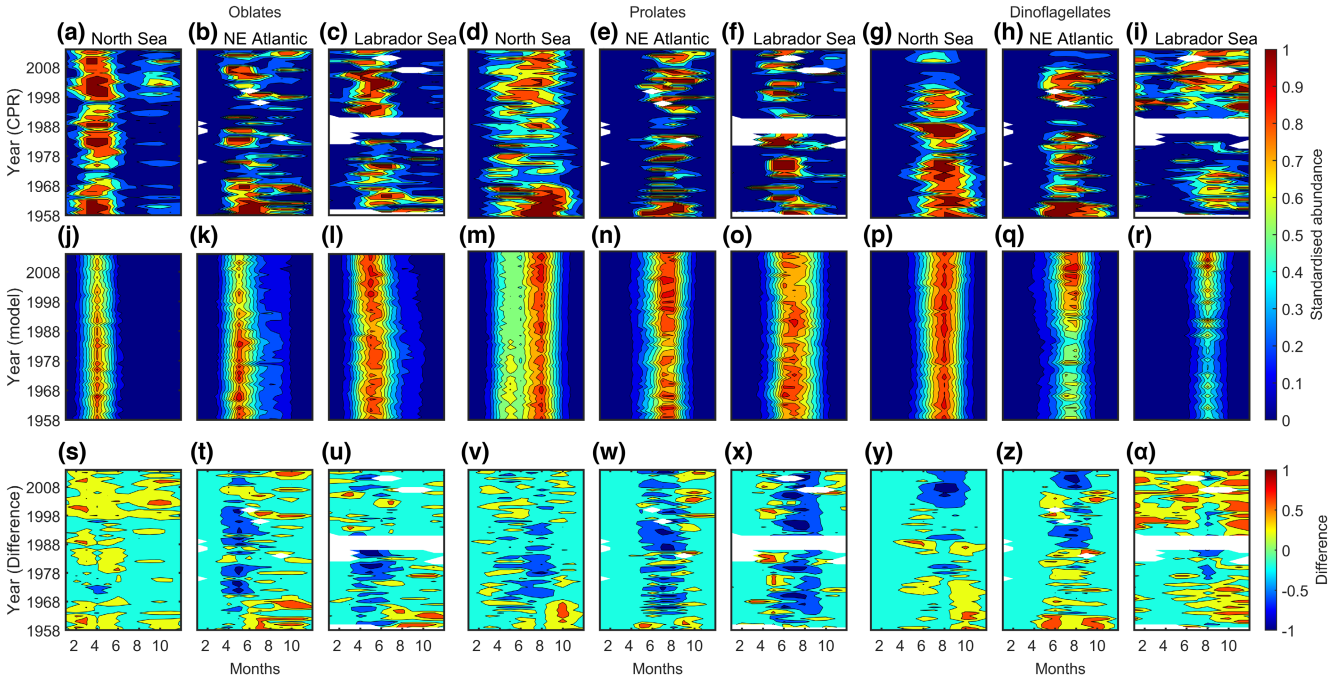

FIGURE 1 Comparisons between observed and modelled long-term monthly abundance of the three taxonomic groups (oblates, prolates and dinoflagellates). (a–i) Long-term changes in the monthly abundance of (a–c) oblates, (d–f) prolates and (g–i) dinoflagellates in the North Sea (a, d and g), the North-East Atlantic (b, e and h) and the Labrador Sea (c, f and i). (j–r) Modelled long-term changes in the monthly abundance of (j–l) oblates, (m–o) prolates and (p–r) dinoflagellates in the North Sea (j, m and p), the North-East Atlantic (k, n and q) and the Labrador Sea (l, o and r). Differences between observed and modelled mean monthly abundance of (s–u) oblates, (v–x) prolates and (y–α) dinoflagellates in the North Sea (s, v and y), the North-East Atlantic (t, w and z) and the Labrador Sea (u, x and α). In a–r, colours denote the mean monthly observed or modelled abundance of a taxonomic group. The abundance in each panel was standardised between 0 and 1 for comparison purpose (Section 2). Spearman correlation coefficients between observed and modelled abundance are displayed in Table 1. In (s–α), colours denote the difference between observed and modelled abundance, red and blue colours indicating an underestimation and an overestimation of the modelled abundance, respectively. Modelled abundances are the average based on the six Earth System Models (ESMs).

$$N_m^* = \frac{N_m}{P90_m} \quad (2)$$

With N_m^* the standardised monthly abundance of a taxonomic group for month m, N_m the monthly abundance for month m and $P90_m$ the 90th percentile of the monthly abundance of the taxonomic group. In rare cases, standardised monthly abundance above 1 were fixed to 1. We chose to use the 90th percentile here instead of the maximum abundance value (as in Equation 1) because the latter would have been too sensitive to outliers that may originate from multiple causes (e.g. exceptional abundance, patchiness or abundance misestimated from only 3 m^3 of seawater filtered; see Figure S1).

2.2 | CMIP6 climate simulations 1850–2100

Species responses to environmental variability were modelled using three environmental variables known to influence phytoplankton phenology at high latitudes (Beaugrand & Kirby, 2018; Boyce et al., 2017; Caracciolo et al., 2021; Lewandowska & Sommer, 2010; Miller, 2004): that is sea surface temperature (SST; °C), surface downwelling shortwave radiation (SDSR; $W m^{-2}$) and dissolved nitrate concentration ($mol m^{-3}$). Climate projections for the three variables originated from the Coupled Model Intercomparison Project Phase 6 (CMIP6; Eyring et al., 2016) and were obtained from the Earth System Grid Federation. We used the shared socioeconomic pathways (SSP) 2–4.5 and 5–8.5 corresponding, respectively, to a medium and a high radiative forcing by 2100 (4.5 and 8.5 $W m^{-2}$; O'Neill et al., 2016, 2017). The simulations of six different ESMs (i.e. CNRM-ESM2-1, GFDL-ESM4, IPSL-CM6A-LR, MPI-ESM1-2-LR, NorESM2-LM and UKESM1-0-LL) covering the time period 1850–2014 (historical simulation) and 2015–2100 (future projections for the two SSP scenarios) were used. An historical perspective is important to better understand the magnitude of the present and future shifts (Beaugrand et al., 2015). The six ESMs were chosen on the basis of data availability for 1850–2100 and the two warming scenarios. All the data were interpolated into daily on a 0.5×0.5° regular grid. Key references (i.e. DOI and dataset version) are provided in Text S1. Long-term projected changes of the three variables, for the six models, the two scenarios and the three regions are displayed in Figures S2–S4.

2.3 | The MacroEcological Theory on the Arrangement of Life

A framework from the MacroEcological theory on the arrangement of life (METAL) theory was used to investigate past, contemporary and future phenological changes in the three taxonomic groups. METAL is a theory that attempts to explain how biodiversity, from the individual to the community level, is organised in space and time and how it responds to environmental changes (Beaugrand, 2015). Based on the concept of the ecological niche sensu Hutchinson (i.e. the set of conditions enabling a species to growth and reproduce; Hutchinson, 1957), one fundamental assumption of METAL is that the niche–environment interaction is a fundamental interaction that enables one to unify and predict a large number of ecological and biogeographical phenomena, as well as the effect of climate-induced environmental changes on individuals, species and communities (Beaugrand, 2015; Beaugrand & Kirby, 2016, 2018). More information on METAL can be found in https://biodiversite.macroecologie.climat.cnrs.fr/. Recently, it has been shown that a framework originating from METAL and using the data collected by the CPR survey could also explain phytoplankton phenology and the resulting annual plankton succession in the North Sea, based on SST, SDSR and nitrate concentration (Caracciolo et al., 2021). By creating a local pseudo-community, composed of fictive species (i.e. pseudo-species), it was possible to reconstruct at a species-level phytoplankton phenology and at a community level the annual plankton succession (Caracciolo et al., 2021). We therefore applied the same framework here to explore how diatom (oblate and prolate) and dinoflagellate phenology might be modified in the coming decades with global climate change.

2.4 | Niche characterisation

We first estimated daily climatologies (based on 365 days) of the three environmental variables described above (i.e. SST, SDSR and nitrate concentration) for three time periods (1958–1976, 1977–1995 and 1996–2014 i.e. 365 days × 3 = 1095 days), three oceanic regions (North Sea, North-East Atlantic and Labrador Sea) and based on six ESMs (i.e. CNRM-ESM2-1, GFDL-ESM4, IPSL-CM6A-LR, MPI-ESM1-2-LR, NorESM2-LM and UKESM1-0-LL). The daily climatologies were then visually compared against the observations originating from the ERA5 dataset (for SST and SDSR; https://cds.climate.copernicus.eu/cdsapp#!/dataset/reanalysis-era5-pressure-levels?tab=overview) and the World Ocean Atlas (for nitrate concentration; https://www.ncei.noaa.gov/products/world-ocean-atlas). For SST and SDSR, because of data availability, daily means were estimated in the three regions between 1959 and 2014 and then converted into daily climatologies for the three time periods (1959–1976, 1977–1995 and 1996–2014). For nitrate concentration, a monthly climatology for the time period 1955–2017 was downloaded from the World Ocean Atlas and a mean was then calculated over the three oceanic regions. Comparisons between observed and reconstructed climatologies from the six ESMs in the North Sea, the North-East Atlantic and the Labrador Sea are displayed in Figures S5, S6 and S7, respectively.

Then, we generated a set of 1,755,000 pseudo-species (i.e. fictive species) and we calculated their abundance along the daily climatologies using a three-dimensional Gaussian niche (Caracciolo et al., 2021):

$$B = c e^{-\frac{1}{2}\left[\left(\frac{x_1 - x_{opt}}{t_1}\right)^2 + \ldots + \left(\frac{x_n - x_{optn}}{t_n}\right)^2\right]} \quad (3)$$

with B the abundance of a pseudo-species along a given environmental gradient x, c the maximum abundance of a pseudo-species (here c was fixed to 1), x_1 to x_n the environmental gradients, with $n = 3$ (SST, SDSR and nitrate concentration). x_{opt1} to x_{optn} are the ecological niche optima along x_1 to x_n and t_1 to t_n the niche amplitude along x_1 to x_n. Niche optima were defined for SST from 0 to 25°C every 1°C, for SDSR from 0 to 400 W m^{-2} every 40 W m^{-2} and for nitrate concentration from 0.001 to 0.05 mol m^{-3} every 0.005 mol m^{-3}. Niche amplitudes were defined for SST from 1 to 10°C every 2°C and for nitrate concentration from 0.001 to 0.015 mol m^{-3} every 0.001 mol m^{-3}. Amplitudes for SDSR were defined as followed: 1, 3, 5, 8, 10, 15, 20, 50 and 100 W m^{-2}. Each pseudo-species was therefore defined by a unique combination of optima and amplitudes along the three environmental gradient, that is by a unique niche, according to the principle of competitive exclusion (Gause, 1934; Hutchinson, 1978). Therefore, the total number of pseudo-species (1,755,000) corresponds to the total number of unique combinations. Niche intervals were chosen to optimise computational cost while covering the largest set of combinations.

We compared the modelled and observed (CPR) abundance at a species and a group (oblates, prolates and dinoflagellates) level. At a species level, we calculated the mean absolute error (MAE) between the daily abundance climatology (based on 365 days × 3 temporal periods = 1095 days) of each species and each of the 1,755,000 pseudo-species we created, for each oceanic region and ESM. Some species exhibited erratic short peaks that were difficult to explain in some regions. To prevent our model to be influenced by these events that might be related to misidentification, CPR silk contamination or species expatriation (i.e. species occurring in unsuitable environmental conditions because of their passive drift induced by oceanic currents; Pulliam, 2000; van der Spoel, 1994), we only summed MAEs from the regions where a given species had a standardised abundance greater than 0.1 during more than 90 days. The use of different thresholds did not alter our conclusions substantially. Finally, for each ESM, we chose a pseudo-species to represent an observed species when it has the lowest MAE in the three regions (Figure 2a–c and Table S2). Therefore, the 44 species may be characterised by different pseudo-species from one ESM to another. This allowed us to examine inter-ESM variability (Figures S2–S7) and the uncertainty associated with the characterisation of a species niche, but also to create a unique bias correction for each ESM. Relationships between modelled and observed daily abundance species climatologies in each region were examined by means of a Spearman rank correlation (Figure 2d–f and Tables S3–S5).

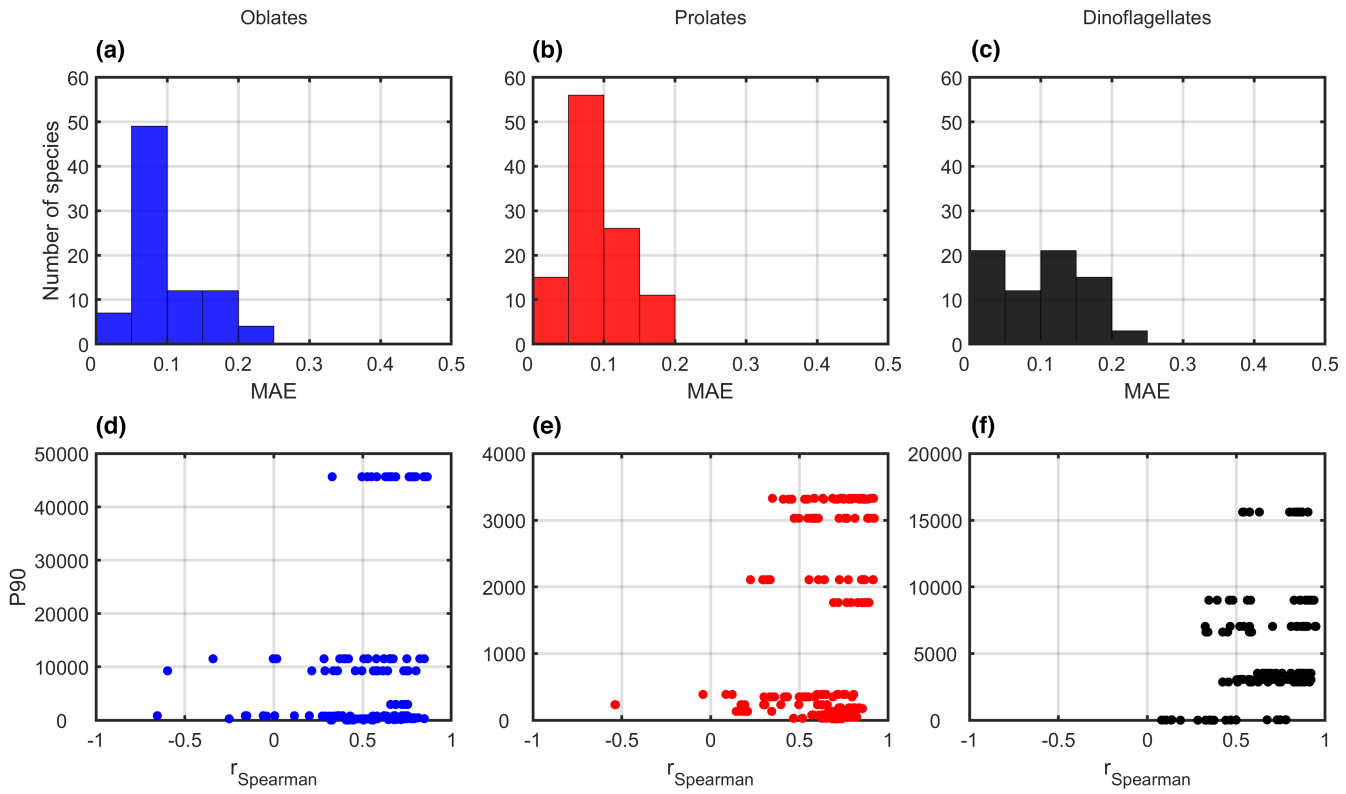

FIGURE 2 Model performance. (a–c) Distribution of the mean absolute errors (MAEs) calculated between observed and modelled abundances of each species/taxa for (a) oblates (blue bars), (b) prolates (red bars) and (c) dinoflagellates (black bars) in the three oceanic regions. (d–f) Relationships between the Spearman rank correlation ($r_{Spearman}$) calculated between the observed and the modelled abundances, and the corresponding 90th percentile of the abundance (P90; see Table S1) values for (d) oblates (blue dots), (e) prolates (red dots) and (f) dinoflagellates (black dots) in the three oceanic regions. Displayed MAEs and Spearman rank correlations were calculated for each Earth System Model (ESM) (see Tables S2–S5). Comparison between the modelled abundance forced by the six ESMs and the observed abundance by the Continuous Plankton Recorder (CPR) survey are shown in Animations S1–S3. Mean monthly observed and predicted standardised abundances of the three taxonomic groups in the three oceanic regions are shown in Figure 1.

To assess whether the use of climatologies based on three temporal periods (1958–1976, 1977–1995 and 1996–2014) might influence model skill and performance, we also estimated the MAEs between the observed and modelled daily abundance climatologies based on a single (1958–2014) and two temporal periods (1958–1985 and 1986–2014; Figures S8 and S9).

2.5 | Long-term changes in the abundance of the three taxonomic groups

Daily abundances of the 44 species were estimated from Equation (3) between 1850 and 2100, using environmental variables assessed from the six models and for the two scenarios (Section 2.4 above). To assess the mean abundance of each group, we weighted species abundance using their P90 (Section 2.1 and Table S1) to account for species contemporary difference in abundance within the three groups (oblates, prolates and dinoflagellates). We used the 90th percentile instead of the maximum abundance value because the latter would have been too sensitive to outliers that may originate from multiple causes (e.g. exceptional abundance, patchiness or abundance misestimated from only 3 m^3 of seawater filtered). Predicted abundances were finally standardised between 0 (the lowest abundance) and 1 (the highest) for each taxonomic group, all ESMs and scenarios as follows:

$$D_m^* = \frac{D_{(m)} - \min(D)}{\max(D) - \min(D)} \quad (4)$$

with D_m^* the standardised predicted abundance of a group for a given ESM, scenario and month m, D_m the predicted abundance for month m and $\min(D)$ and $\max(D)$ the minimal and maximal predicted abundance between 1850 and 2100 in a given oceanic region, respectively. Finally, the relationships between modelled and observed standardised monthly abundances were quantified for 1958–2014 (i.e. overlapping period of observed and modelled data) using the Spearman correlation coefficient (Figure 1a–r and Table 1). Differences between observed and modelled standardised monthly abundances were also calculated to compare the seasonal and long-term trends (Figure 1s–α).

To test whether the long-term changes in phenology and abundance of the three groups were well modelled by our approach, we also estimated the annual (long-term changes) and monthly (seasonal variations) average of the modelled and observed abundances of the three groups in the three regions, between 1958 and 2014 (Figures S10 and S11). Annual and monthly patterns were

subsequently compared by means of a Spearman rank correlation coefficient (Tables S6 and S7).

2.6 | Long-term phenological changes in the three taxonomic groups

We examined phenological shifts of the three taxonomic groups between 1850 and 2100, for the two scenarios and the six ESMs in the three regions. Average daily abundances of each group were smoothed by means of a 15-order moving average (i.e. time scale covering a month) and then, for each year between 1850 and 2100, we estimated six phenological indices: that is (1) maximum annual abundance (MAA), (2) the day where MAA is reached, (3) initiation and (4) termination of the seasonal reproductive period (SRP), that is the first and the last days where the abundance is ≥50% of MAA, (5) seasonal duration, that is the number of consecutive days where abundance is ≥50% of MAA, and (6) integrated MAA (IMAA) (Figure 3). The six indices were calculated for each taxonomic group, all models, scenarios and North Atlantic regions. Bimodality (i.e. two population peaks within a single year) was sometimes observed for the diatoms in the three regions, but as this pattern fluctuated in time (i.e. short erratic peaks) and was not well reproduced by all ESMs, when a bimodality was observed we only considered the peak with the highest abundance. An average of the results of the six ESMs was then calculated for 1850–2100 for each scenario and North Atlantic region (Figures 4–6). In addition, we focussed on three decades: 1850–1859, 2000–2009 and 2090–2099. For these decades, we assessed the inter-model average and the associated standard deviation of each index (mean ± uncertainty; Tables S8–S16; Kwiatkowski et al., 2020).

3 | RESULTS

Visual comparisons between observed and reconstructed SST, SDSR and nitrate concentration showed that the seasonal cycle and the long-term trend of each variable was in general well reconstructed by the ESMs in the three oceanic regions and for the three time periods (except for nitrate long-term trend, see Section 2 and Figures S5–S7).

3.1 | Model performance

Model performance was first assessed by visually comparing the observed and modelled daily abundance of each species for the three periods and North Atlantic regions (Animations S1–S3). The phenology of most species was well modelled by our approach and the MAE between the observed and modelled abundance was generally low (below 0.1 for diatoms and below 0.2 for dinoflagellates; Figure 2a–c and Table S2; see Section 2). MAEs calculated between observed and modelled abundance based on a single (1958–2014) or two temporal periods (1958–1985 and 1986–2014) climatologies were higher, indicating that our model performed better when based on the three temporal periods climatologies (Figures S8 and S9). We then estimated the Spearman rank correlation coefficient between daily observed and modelled patterns, which revealed that for most species, correlations were highly positive (Figure 2d–f and Tables S3–S5). A few low correlations were observed, however, indicating that for some species our approach did not work well in some North Atlantic regions and for some ESMs. Low correlations between observations and model reconstructions may be caused by some regional hydro-meteorological events that are not well reproduced by an ESM or by some methodological limitations of our approach (see Section 4). However, their weight in the subsequent analyses was low, as shown by the value of their P90 (i.e. the 90th percentile of their abundance, Section 2, Figure 2d–f and Table S1); the higher the P90, the higher the abundance of a species in a North Atlantic region and therefore the greater its weight in subsequent analyses at the group level (Figures 4–6).

Modelled species abundances were finally aggregated at a monthly scale for each group (oblates, prolates and dinoflagellates) by weighting the abundance of each species according to the value of their P90 (Table S1). A monthly scale was first chosen for comparison of the modelling approach with the in situ monthly observations collected by the CPR survey, whom sampling is carried out at a monthly interval (Richardson et al., 2006). Differences between observed and modelled long-term changes in monthly abundance showed that model performance varied greatly among regions and species groups, mostly because of the nature of the CPR data (i.e. large variability in observed abundance; see Figure 1a–i versus Figure 1j–r and Section 4) and because the reconstructed climatic variability was not supposed to exactly match the variability that was observed between 1958 and 2014 (Stock et al., 2011). On the contrary, Spearman rank correlations calculated between observed and modelled mean monthly abundances were all positively correlated significantly, although the correlations were statistically more significant in the North Sea and the North-East Atlantic than in the Labrador Sea (Spearman rank correlations coefficient between 0.7 and 0.83 in the North Sea, 0.64 and 0.73 in the North-East Atlantic, and 0.5 and 0.58 in the Labrador Sea; Figure 1 and Table 1). The comparison between long-term changes in the annual abundance of prolates in the three regions, of oblates in the North-East Atlantic and of oblates and dinoflagellates in the Labrador Sea were globally

TABLE 1 Spearman rank correlations between long-term changes in observed and modelled monthly abundance of the three taxonomic groups (oblates, prolates and dinoflagellates) in the three studied regions.

	North Sea	North-East Atlantic	Labrador Sea
Oblates	0.70	0.64	0.55
Prolates	0.79	0.73	0.58
Dinoflagellates	0.83	0.72	0.50
Degree of freedom	684	677	600

Note: All correlations were significant ($p < .01$). The degree of freedom associated with each oceanic region is also indicated. Long-term monthly changes in observed and modelled abundance are displayed in Figure 1.

well reconstructed (Figure S10), but the correlations were not always significant, suggesting that some periods and years did not match well (Table S6). On the contrary, our model did not fully reconstruct the long-term trends in oblates and dinoflagellates in the North Sea and of dinoflagellates in the North-East Atlantic (Figure S10), which was confirmed by Spearman rank correlations (Table S6). Such difficulties to explain observed long-term changes in abundance were expected since ESMs are known to have some difficulties to reconstruct high-frequency natural variability in climate well (Stock et al., 2011). Finally, the comparison between observed and modelled monthly changes in abundance revealed that the seasonal cycles of the three groups in the three regions were correctly reconstructed (significant Spearman rank correlations above 0.85; Figure S11 and Table S7).

3.2 | Phenological shifts in the North Atlantic

In the North Atlantic Ocean, phenological shifts projected by our models were relatively moderate for 1850–1950 (Figures 4–6). Major changes were expected to occur from the end of 1970s onwards when the rate of ocean warming increased and led to an increase in water column stratification (IPCC, 2019; see also Figures S2–S4). A decline in oblate abundance was generally observed under both scenarios in the three regions, associated with a reduction in their SRP, whereas an increase in prolate and dinoflagellate abundance was projected, associated with an expansion of their SRP (Figures 4–6). Expectedly, the magnitude of the projected changes in phenology and abundance appeared to be more important under the high warming scenario (Figures 4–6).

3.3 | Phenological shifts in the North Sea

In the North Sea (Figure 4a), modelled long-term daily phenological changes exhibited similar patterns for both SSP scenarios, with a shift in the diatom community composition, although changes were highest under SSP5-8.5 (Figure 4b–q). Oblate diatoms are expected to decline, the MAA decreasing from 1671.1 ± 494.7 cells per CPR sample in 1850–1859 to 1176.9 ± 573.2 or 785.1 ± 347.7 cells per CPR sample in 2090–2099 for scenarios SSP2-4.5 and SSP5-8.5, respectively (Figure 4b,e and Table S8). In contrast, prolate MAA rose from 302 ± 53.3 cells per CPR sample in 1850–1859 to 360.5 ± 77.5 or 392.6 ± 115.5 cells per CPR sample in 2090–2099 for SSP2-4.5 and SSP5-8.5, respectively (Figure 4c,f and Table S9). No significant changes in the duration of the SRP were found for both groups (Figure 4h–i and Tables S8 and S9), although they exhibit an earlier and a later (both initiation and termination) phenology, respectively (Figure 4j–k,m–n and Tables S8 and S9). These phenological shifts were accompanied by a shift in their IMAA, our results suggesting that oblates may experience a strong decrease from 390 ± 92.8 cells per CPR sample in 1850–1859 to 283.8 ± 97.4 or 192 ± 59 cells per CPR sample in 2090–2099 for scenarios SSP2-4.5 and SSP5-8.5, respectively. An opposite pattern is predicted for prolates, although it may be less important (from 122.8 ± 32.7 cells per CPR sample in 1850–1859 to 134.5 ± 18.6 or 148.8 ± 30.1 cells per CPR sample in 2090–2099 for SSP2-4.5 and SSP5-8.5, respectively; Figure 4p–q and Tables S8 and S9).

Modelled changes in dinoflagellates exhibited a phenological expansion. Their MAA remained constant throughout the period, although they decreased at the very end of the century under SSP5-8.5 from 2853.9 ± 336.3 cells per CPR sample in 1850–1859 to 2599.3 ± 553.2 in 2090–2099 (Figure 4d,g and Table S10). The duration of their SRP is expected to rise throughout the 21st century (from a mean of 103 ± 16 days in 1850–1859 to 107 ± 6 days in 2000–2009 and to 127 ± 13 or 143 ± 25 days in 2090–2099 under SSP2-4.5 and SSP5-8.5, respectively; Figure 4h–i and Table S10) with both an earlier initiation and a later termination of their SRP (Figure 4l,o and Table S10), associated with an increase in their IMAA (Figure 4p–q and Table S10).

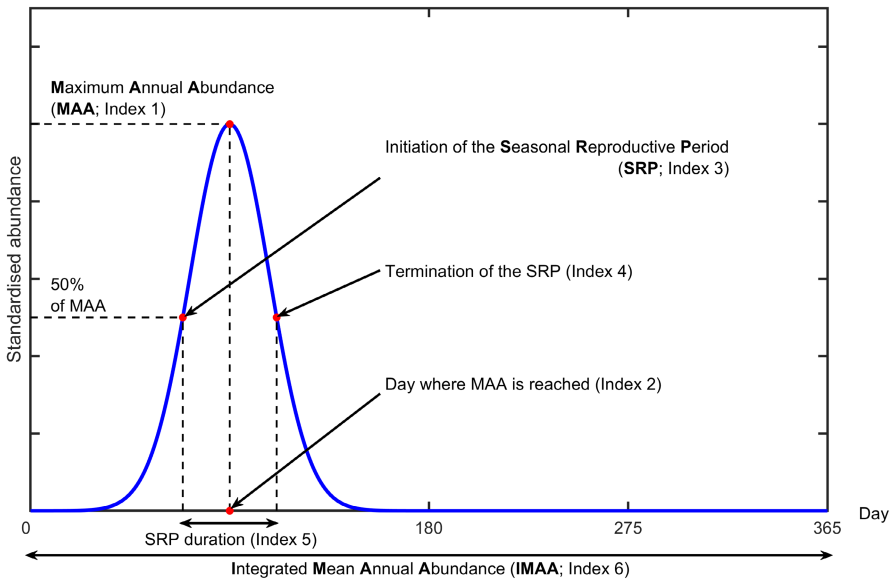

FIGURE 3 Theoretical diagram explaining graphically the six phenological indices used in this study. Six phenological indices were defined: the Maximum Annual Abundance (MAA; Index 1), the day where MAA is reached (Index 2), the initiation (Index 3) and the termination (Index 4) of the Seasonal Reproductive Period (SRP), that is the first and the last days where the abundance is ≥50% of MAA, the seasonal duration (Index 5), that is the number of consecutive days where abundance is ≥50% of MAA, and the Integrated Mean Annual Abundance (IMAA; Index 6).

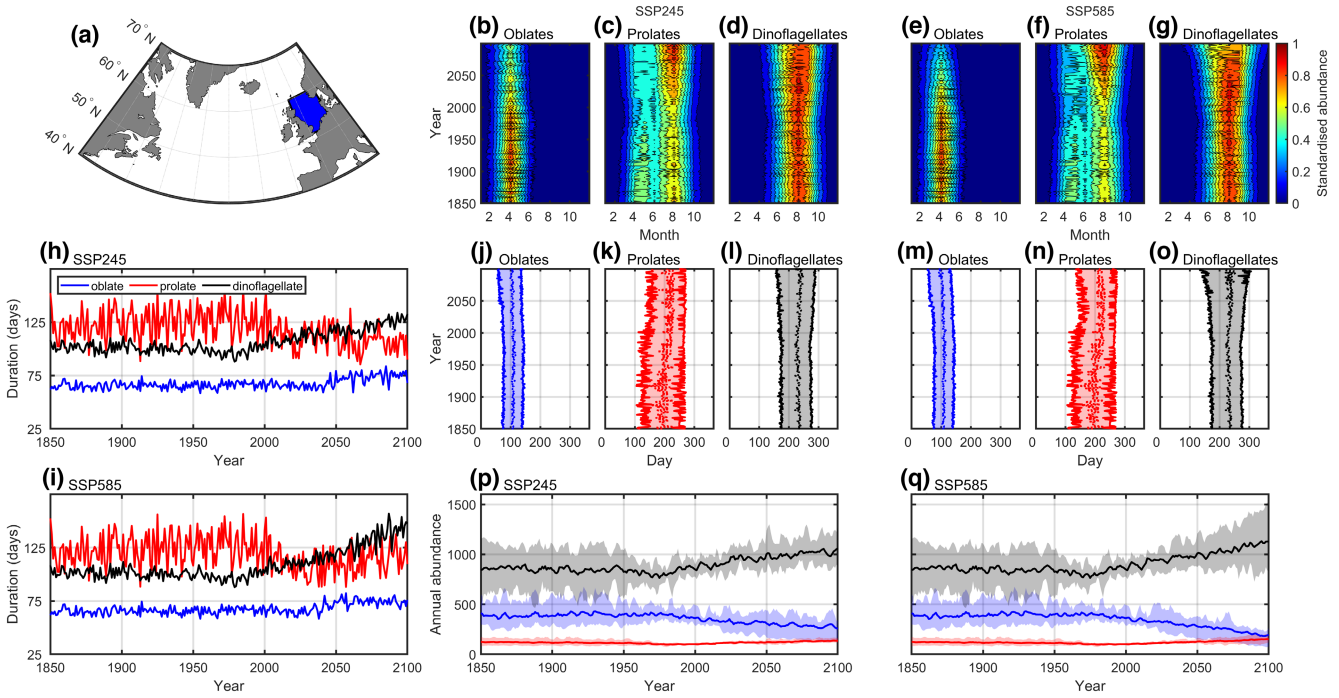

FIGURE 4 Modelled long-term phenological changes in diatoms and dinoflagellates in the North Sea (1850–2100). (a) Spatial distribution of Continuous Plankton Recorder (CPR) survey sampling. (b–g) Long-term monthly changes in the standardised abundance of (b and e) oblates, (c and f) prolates and (d and g) dinoflagellates for scenarios (b–d) SSP2-4.5 and (e–g) SSP5-8.5. Each panel was standardised between 0 and 1. Colours denote the mean monthly standardised abundance of a taxonomic group. (h–i) Long-term annual changes in phenology duration for scenarios (h) SSP2-4.5 and (i) SSP5-8.5. (j–o) Long-term changes in the initiation and termination of the Seasonal Reproductive Period (SRP) for (j and m) oblates, (k and n) prolates and (l and o) dinoflagellates. In each panel, the first and last tick line denotes the initiation and the termination day of the SRP. Shading denotes the duration of the SRP and the dotted line displays the day where Maximum Annual Abundance (MAA) is reached. (p–q) Long-term changes in Integrated Mean Annual Abundance (IMAA; cell per CPR sample) for scenarios (p) SSP2-4.5 and (q) SSP5-8.5. The shade denotes the minimum and maximum mean abundance estimated from the environmental variables originating from the six Earth System Models (ESMs). In (h–q) oblates are in blue, prolates in red and dinoflagellates in black. In (b–q), each index corresponds to the mean of the six ESMs. The meaning of the six phenological indices is summarised in Figure 3.

3.4 | Phenological shifts in the North-East Atlantic

In the North-East Atlantic region (Figure 5a), phenological shifts were also predicted by our approach, the magnitude of which depending on warming intensity (Figure 5b–q). Oblate MAA decreased after the end of the 20th century, whereas prolate MAA rose circa 2050 under both scenarios (Figure 5b,c,e,f, Tables S11 and S12). Oblates underwent a phenological contraction from 76±22 days in 2000–2009 to 69±14 or 64±15 days in 2090–2099 for SSP2-4.5 and SSP5-8.5, respectively (Figure 5h–i and Table S11), accompanied by an earlier initiation in their SRP (Figure 5j,m and Table S11). In contrast, prolates exhibited a strong phenological dilatation from 91±6 days in 2000–2009 to 110±11 or 119±22 days in 2090–2099 for scenarios SSP2-4.5 and SSP5-8.5, respectively (Figure 5h–i and Table S12), with an earlier initiation and a later termination of their SRP (Figure 5k,n and Table S12). At the end of the century, they reached earlier their MAA in the year, that is around day number 204±16 or 197±19 in 2090–2099 for scenarios SSP2-4.5 and SSP5-8.5, respectively, in comparison to day 215±4 in 1850–1859 (Figure 5k,n and Table S12). Oblate IMAA remained constant under scenario SSP2-4.5 but decreased under SSP5-8.5. Prolate IMAA slightly increased under both scenarios but remained below the value observed for oblates (Figure 5p–q and Tables S11 and S12).

Dinoflagellates also underwent a phenological expansion, associated with an increase in their MAA throughout the 21st century (Figure 5d,g and Table S13), a longer duration (Figure 5h–i and Table S13) caused by an earlier initiation (around day number 215±4 in 1850–1859 and 204±16 or 197±19 for SSP2-4.5 and 5–8.5, respectively) and a later termination (around day number 254±9 in 1850–1859 and 262±5 or 268±9 in 2090–2099 for scenarios SSP2-4.5 and SSP5-8.5, respectively, Table S13) of their SRP. Their IMAA rose above those of oblates during the first half of the 21st century, although there was a high inter-model variance (Figure 5p–q and Table S13).

3.5 | Phenological shifts in the Labrador Sea

In the Labrador Sea (Figure 6a), distinct phenological shifts were found, also depending on the SSP scenarios (Figure 6b–q). Under scenario SSP2-4.5, oblates exhibited a slight increase

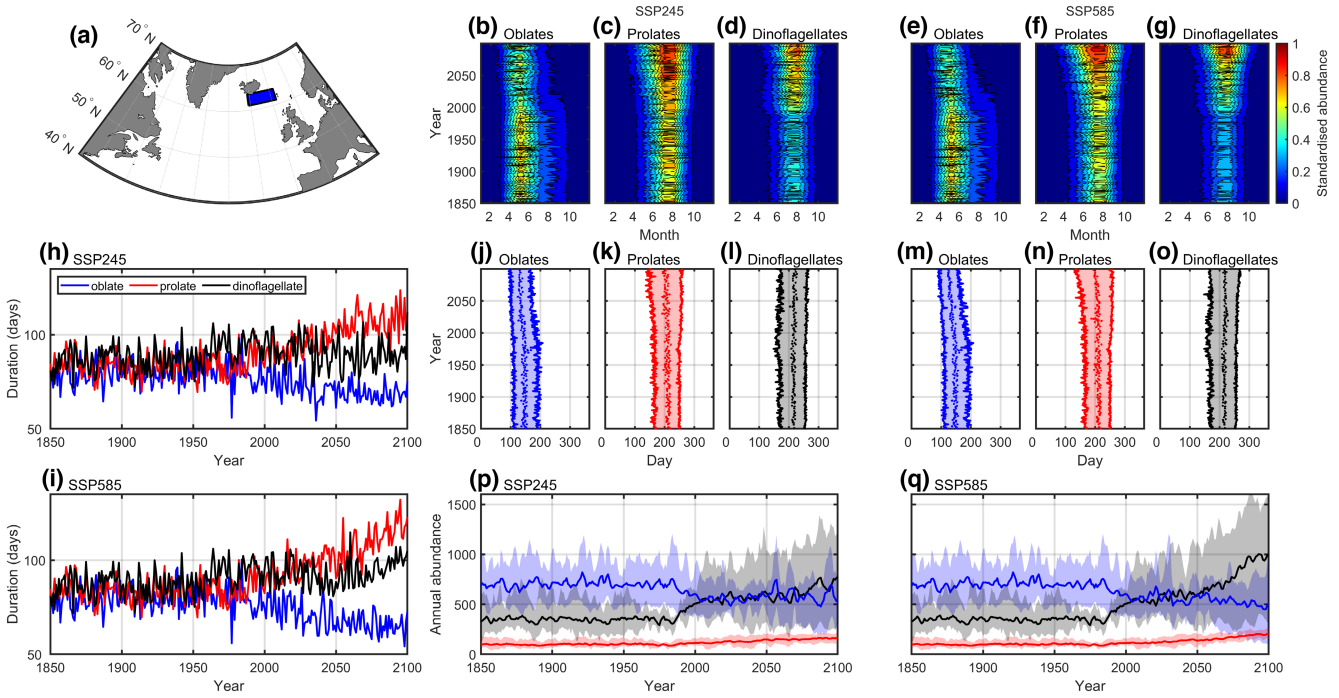

FIGURE 5 Modelled long-term phenological changes in diatoms and dinoflagellates in the North-East Atlantic (1850–2100). (a) Spatial distribution of Continuous Plankton Recorder (CPR) sampling. (b–g) Long-term monthly changes in the standardised abundance of (b and e) oblates, (c and f) prolates and (d and g) dinoflagellates for scenarios (b–d) SSP2-4.5 and (e–g) SSP5-8.5. Each panel was standardised between 0 and 1. Colours denote the mean monthly standardised abundance of a taxonomic group. (h–i) Long-term annual changes in phenology duration for scenarios (h) SSP2-4.5 and (i) SSP5-8.5. (j–o) Long-term changes in the initiation and termination of the Seasonal Reproductive Period (SRP) for (j and m) oblates, (k and n) prolates and (l and o) dinoflagellates. In each panel, the first and last tick line denotes the initiation and the termination day of the SRP. Shading denotes the duration of the SRP and the dotted line displays the day where Maximum Annual Abundance (MAA) is reached. (p–q) Long-term changes in Integrated Mean Annual Abundance (IMAA; cell per CPR sample) for scenarios (p) SSP2-4.5 and (q) SSP5-8.5. The shade denotes the minimum and maximum mean abundance estimated from the environmental variables originating from the six Earth System Models (ESMs). In (h–q) oblates are in blue, prolates in red and dinoflagellates in black. In (b–q), each index corresponds to the mean of the six ESMs. The meaning of the six phenological indices is summarised in Figure 3.

in their MAA (i.e. 3770.1 ± 769.1 cells per CPR sample in 2000–2009 versus 4055.5 ± 545.4 cells per CPR sample in 2090–2099; Table S14), although the duration of their SRP slightly diminished from 87 ± 11 days in 2000–2009 to 84 ± 13 days in 2090–2099 (Figure 6h,j and Table S14). Prolates maintained both their MAA and IMAA throughout the period 1850–2100 (Figure 6c,p and Table S15), the most significant changes occurring in the duration of their SRP (from 97 ± 31 days in 2000–2009 to 107 ± 36 in 2090–2099; Figure 6h and Table S15) accompanied by an earlier phenology (Figure 6k and Table S15). Dinoflagellates should exhibit a large increase in their MAA, especially after 2050, from 910 ± 428.4 cells per CPR sample in 2000–2009 to 1914.4 ± 1125.2 in 2090–2099 (Figure 6d and Table S16) without a significant increase in the duration of their SRP (Figure 6h and Table S16) or a change in initiation or termination (Figure 6l and Table S16). Their IMAA slightly increased but remained above that of oblates (Figure 6p and Tables S14 and S16).

Under SSP5-8.5, our approach predicted a shift from a system dominated by oblates to a system dominated by dinoflagellates (Figure 6b–q). The oblates exhibited a decrease in their MAA from 3770.1 ± 769.1 cells per CPR sample in 2000–2009 to 3184.4 ± 727.2 in 2090–2099 (Figure 6e and Table S14), accompanied by a decrease in the duration of their SRP from 86.9 ± 10.5 days in 2000–2009 to 72.8 ± 8.3 days in 2090–2099 (Figure 6i and Table S14), and an earlier initiation (Figure 6m and Table S14). Their IMAA sharply decreased, especially during the second half of the 21st century, from 1077.1 ± 178.6 cells per CPR sample in 2000–2009 to 777.9 ± 245.5 in 2090–2099 (Figure 6q and Table S14). No changes were found for prolate MAA (Figure 6f and Table S15) but their SRP lasted longer, from 97 ± 31 days in 2000–2009 to 115 ± 35 in 2090–2099 (Figure 6i,n and Table S15). Their IMAA was low under this scenario (Figure 6p–q and Table S15). Dinoflagellate shifts were amplified, their MAA increased substantially, from 910 ± 428.4 cells per CPR sample in 2000–2009 to 2898.2 ± 1052.0 in 2090–2099 (Figure 6g and Table S16). These changes were more prominent at the end of the 21st century, from 66 ± 12 days in 2000–2009 to 82 ± 18 in 2090–2099 (Figure 6i and Table S16), resulting in a phenological dilatation (Figure 6o and Table S16). Their IMAA tripled between the beginning and the end of the 21st century, from 204.5 ± 66.9 cells per CPR sample in 2000–2009 to 738.8 ± 319.3 in 2090–2099 (Table S16), resulting in a shift from oblates to dinoflagellates. As the long-term phenological changes in the three groups were more difficult to reconstruct in this region (Table 1), our predictions should be considered with degree of caution.

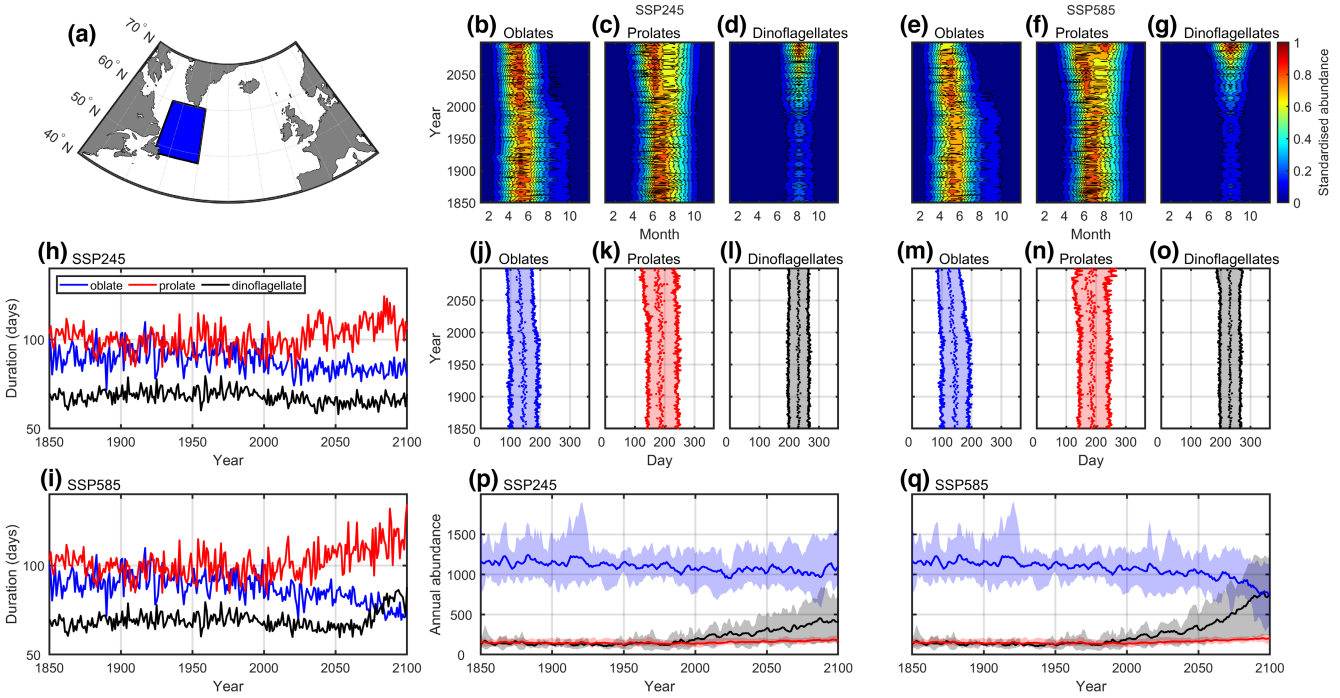

FIGURE 6 Modelled long-term phenological changes in diatoms and dinoflagellates in the Labrador Sea (1850–2100). (a) Spatial distribution of Continuous Plankton Recorder (CPR) sampling. (b–g) Long-term monthly changes in the standardised abundance of (b and e) oblates, (c and f) prolates and (d and g) dinoflagellates for scenarios (b–d) SSP2-4.5 and (e–g) SSP5-8.5. Each panel was standardised between 0 and 1. Colours denote the mean monthly standardised abundance of a taxonomic group. (h–i) Long-term annual changes in phenology duration for scenarios (h) SSP2-4.5 and (i) SSP5-8.5. (j–o) Long-term changes in the initiation and termination of the Seasonal Reproductive Period (SRP) for (j and m) oblates, (k and n) prolates and (l and o) dinoflagellates. In each panel, the first and last tick lines denote the initiation and the termination day of the SRP. Shading denotes the duration of the SRP and the dotted line displays the day where Maximum Annual Abundance (MAA) is reached. (p–q) Long-term changes in Integrated Mean Annual Abundance (IMAA; cell per CPR sample) for scenarios (p) SSP2-4.5 and (q) SSP5-8.5. The shade denotes the minimum and maximum mean abundance estimated from the environmental variables originating from the six Earth System Models (ESMs). In (h–q), oblates are in blue, prolates in red and dinoflagellates in black. In (b–q), each index corresponds to the mean of the six ESMs. The meaning of the six phenological indices is summarised in Figure 3.

4 | DISCUSSION

Some discrepancies between modelled and observed abundance indicate that our model may have some limitations (Figure 1, Figures S10 and S11 and Animations S1–S3). For example, the decrease in the abundance of dinoflagellates in the North Sea and the North-East Atlantic, and the increase of oblates in the North Sea, was not captured well by our approach (Figure 1 and Figure S10). In the same way, the fit between observed and reconstructed daily abundances varied among the three different temporal periods (Animations S1–S3). For example, the abundance of *Leptocylindrus danicus* in the North Sea was correctly reconstructed for the temporal periods 1977–1995 and 1996–2014 but not for 1958–1977 (Animation S1). These inconsistencies may originate from (i) our framework, (ii) the CPR sampling and (iii) the ESMs.

4.1 | Limitations of our approach

In this study, we made a series of choices and assumptions that might have affected model performance. First, we used an approach based on METAL rather than a species distribution model (SDM). This choice was made because we showed previously that METAL correctly reconstructs phytoplankton phenology and annual succession when applied to the CPR data (Caracciolo et al., 2021) while it has been shown that most SDM poorly performed with those data (Brun et al., 2016). In addition, using METAL enables us to convert the monthly CPR observations at a daily scale, which is more adapted (i) to reconstruct/project the long-term phenological changes from 1850 to 2100, (ii) to examine their trends (Henson et al., 2018) and more importantly (iii) to demonstrate that the niche-environment interaction governs long-term phenological phytoplankton shifts (Beaugrand & Kirby, 2018).

Second, we used a symmetric Gaussian function to model the thermal niche of the 44 phytoplanktonic species. Phytoplankton are ectotherms and may therefore have asymmetric thermal niches (Beaugrand et al., 2022; Martin & Huey, 2008; Thomas et al., 2012); in particular, they might be able to tolerate a larger range of cold temperatures (i.e. below their thermal optimum) and a narrower range of warm temperatures (i.e. above their thermal optimum; Martin & Huey, 2008). However, Caracciolo et al. (2021) reconstructed phytoplankton phenology and annual succession well in the

North Sea using symmetrical niches. Furthermore, the use of asymmetrical Gaussian functions would have also increased computational cost. Nevertheless, we acknowledge that the consideration of asymmetrical niches might perhaps improve our results. For example, the existence of an upper thermal limit above which the abundance rapidly declined substantially (e.g. the events observed with the dinoflagellates in the North Sea and the North-East Atlantic; Figure 1g,h and Figure S10c,f) was not reproduced by our model; indeed, the modelled shifts were almost always gradual (Figure 1p–q and Figure S10c,f).

Last, we supposed that species niches will be conserved over the time period 1850–2100 (i.e. the assumption of niche conservatism), an assumption that is generally formulated by modellers that project species response to climate change (Soberon & Nakamura, 2009). The large population size and fast generation time of phytoplankton are supposed to allow a rapid alteration of their niches (Litchman et al., 2012) but some studies (on zooplankton however) have not seen any niche alteration at a decadal scale (Helaouët & Beaugrand, 2007) and there must exist fundamental constraints that limit adaptation (e.g. phytoplankton morphological traits, which affect nutrient uptake, are supposed to be highly conserved; Beaugrand & Kirby, 2018; Kléparski et al., 2022; Litchman et al., 2007).

4.2 | Limitations related to the CPR sampling

Another source of discrepancy between modelled and observed abundance may originate from the sampling by the CPR. First, sampling is carried out at a monthly scale over large areas (Richardson et al., 2006) and it is likely that such a sampling frequency is not always appropriate to properly characterise blooms as phytoplankton exhibits typically a short life cycle. Second, the CPR machine uses a 270 μm mesh silk that mostly collects large armoured dinoflagellates and chain forming diatoms but undersamples smaller phytoplankton species. These sampling biases might explain the large variability observed in the abundance of phytoplankton species, affecting subsequently niche characterisation and modelled reconstructions (Figure 1a–i). However, our results suggest this is not the case for the vast majority of species (Animations S1–S3 and Tables S2–S5). For example, some of the smallest species, for example *Thalassionema nitzschioides* and *Cylindrotheca closterium*, were well modelled in the North Sea and the North-East Atlantic but not in the Labrador Sea (Tables S3–S5 and Animations S1–S3) suggesting that the problem might not be related with a sampling bias affecting model performance. Third, the CPR sampling is heterogeneous in space and time and some regions were not continuously sampled between 1958 and 2014 (Richardson et al., 2006). For example, no CPR sample was available in the Labrador Sea at the end of the 1980s (white bands in Figure 1c,f,i,u,x,α). However, it is thought that the CPR collects an important fraction of the abundance of each taxon and is therefore though to be robust to examine seasonal and interannual patterns (Richardson et al., 2006).

4.3 | Limitations from ESMs

The reconstructed regional climatic variability between 1958 and 2014 by ESMs is not supposed to exactly match the variability that was observed during that time (Stock et al., 2011), a bias that might have also affected niche estimates and that might therefore explain the discrepancies between observed and modelled mean long-term changes in abundance (Figure 1a–r and Figure S10). For example, the abundance of *C. closterium* was well modelled in the North Sea with CNRM-ESM2-1, IPSL-CM6A-LR and NorESM2-LM but not with MPI-ESM1-2-LR, GFDL-ESM4 and UKESM1-0-LL (Table S3). Indeed, there exists large variations in SST, SDSR and nitrate concentration among the six ESMs in some regions (Figures S5–S7). Nevertheless, it should be noticed that our approach consistently modelled the seasonal cycle of the three groups in the three regions and the modelled long-term trends were generally in agreement with the observations, especially for prolates in the three regions, oblates in the North-East Atlantic and oblates and dinoflagellates in the Labrador Sea (Figures S10 and S11 and Tables S6 and S7).

4.4 | Long-term changes in the phenology of diatoms and dinoflagellates

Modelled shifts are in agreement with theoretical projections, that is that spring species (i.e. oblates) experience a phenological contraction and an earlier phenology, whereas late summer species (i.e. prolates and dinoflagellates) exhibit a phenological expansion with both an earlier initiation and a later termination (Beaugrand & Kirby, 2018). The phenological contraction of oblates, associated with a decline in abundance, is indicative of species/taxa that reach the limits of their phenological plasticity (Beaugrand & Kirby, 2018), probably because an earlier phenology in spring is impossible as winter photoperiod and light levels limits primary production at high latitudes (Boyce et al., 2017; Caracciolo et al., 2021) and/or because the decrease in nitrate concentration (Figures S2–S4), which are an essential constituent of proteins and nucleic acids that are, in turn, critical for the synthesis of organic matter (Miller, 2004), limits the size of the bloom. Therefore, these diatoms might encounter more favourable environmental conditions at high latitudes, causing a biogeographical shift, a postulate that would be in agreement with the increased primary production projected by ESMs in the Arctic region (Kwiatkowski et al., 2020) and the observed increase and decrease in diatom populations in the North-Sea and the bay of Biscay, respectively (Edwards et al., 2022). On the contrary, the phenological expansion of prolates and dinoflagellates is indicative of species/taxa that are adapted to the reinforced stratified and nutrient-depleted conditions in the future North Atlantic Ocean (Beaugrand & Kirby, 2018; Kwiatkowski et al., 2020). The elongated cell shape of prolates reduces their sinking speed while not affecting their capacity to uptake nutrients, enabling them to remain in the well-lit upper part of the water column (Kléparski et al., 2022; Padisak et al., 2003).

Furthermore, it has been shown that some taxa belonging to this taxonomic group (e.g. *Rhizosolenia*) were able to passively migrate between the surface layers and the nutricline, enabling them to harvest nutrients more efficiently (Kemp & Villareal, 2013, 2018). Similarly, the dinoflagellates have flagella which enable them to move and actively exploit nutrients in the water column. They are also capable of switching nutritional strategies to mixotrophy when less nutrients are available (Miller, 2004).

Because of the shifts in phytoplankton phenology, changes in species succession are expected to desynchronise species interaction and trigger trophic mismatch (Beaugrand et al., 2003; Cushing, 1990; Edwards & Richardson, 2004). For a given season, mismatch may occur when some species exhibit different range of tolerance for a given environmental variable. Such alterations of the trophodynamics have already been observed in freshwater lakes (Winder & Schindler, 2004) but remain difficult to anticipate in the marine environment because each species has a specific response to environmental variability, which is driven by its life strategy and its niche (Beaugrand & Kirby, 2018). Furthermore, it has also been shown that only seasonally heterogeneous environmental changes can lead to a desynchronisation in species interaction (e.g. warmer temperature in spring but not in summer; Straile et al., 2015). Results from the METAL theory suggest that trophic mismatch might be limited however, because interacting species have at least a part of their ecological niche in common, providing that no other important ecological dimensions or habitat requirements differ among them (Beaugrand & Kirby, 2018). Indeed, species are more expected to track changes along the environmental variables for which they have the narrowest tolerance (Ackerly, 2003). Therefore, in the pelagic environment, one could expect a mismatch among species that are not linked to the same habitat components (i.e. the stable- and substrate-biotope components; van der Spoel, 1994). For example, it has been shown that a shift in phytoplankton phenology is more likely to affect the fish that spawn in geographically fixed areas rather than those that have their spawning grounds moving according to the environmental changes (Asch et al., 2019).

Diatoms and dinoflagellates have been historically separated into two distinct functional types (Kemp & Villareal, 2018; Margalef, 1978). According to Margalef's mandala (Margalef, 1978), diatoms thrive when the water column is poorly stratified and turbulent and when nutrients concentration is relatively high. In contrast, dinoflagellates dominate in stratified conditions and lower nutrients concentration. By simplifying Margalef's framework (Margalef, 1978), a decline in primary production and carbon export (therefore the biological pump; Passow & Carlson, 2012) is anticipated in the North Atlantic because ocean warming will enhance water column stratification and reduce nutrients, which are believed to negatively affect the diatoms as a whole (Bopp et al., 2005; Kemp & Villareal, 2018; Kléparski et al., 2022; Marinov et al., 2010; Tréguer et al., 2018). Our results nuance these projections. Although they show that diatom abundance as a whole will decrease, they also suggest that prolates may indeed persist and increase in a more stratified ocean, albeit probably not to an abundance level that might compensate the large diminution in the abundance experienced by oblates. Indeed, massive blooms of those last diatoms in spring generate high carbon export through the generation of marine snow (Kléparski et al., 2022; Raven & Waite, 2004; Smetacek, 1985) and it is therefore unlikely that the slight increase in prolates will overcome the decrease in carbon exportation induced by the reduction in oblate abundance. Furthermore, the transfer efficiency of carbon to the deep ocean is reduced with smaller sized slow-sinking cells, and therefore the shift from large round oblates to smaller elongated prolates will also diminish the rate of carbon export (Henson et al., 2022). Whether this shift might also affect species aggregation remains an open question as the causes of this phenomenon are not clear (e.g. defence against predation, response to changes in turbulence or buoyancy regulation) (Lürling, 2021; Pančić & Kiørboe, 2018; Smayda, 1970; Sournia, 1982). Our results also suggest that dinoflagellate abundance will rise in the three North Atlantic regions. Although the contribution of this group to the biological pump is poorly understood, a study has shown that dinoflagellate blooms sometimes coincide with a rise in carbon export at an annual scale in the North-East Atlantic at 3000 m (Henson et al., 2012). It has also been shown that the consideration of mixotrophic organisms (e.g. dinoflagellates) within biogeochemical models can increase the flux of carbon export (Ward & Follows, 2016). Therefore, this group might alleviate to some extent the consequences of the reduction in oblates on the biological pump in the North Atlantic, albeit export from the surface ocean is also strongly influenced by synergistic effects such as nutrient delivery through remineralisation or direct inputs, processes that are difficult to predict (Passow & Carlson, 2012).

ESMs used as part of CMIP5 included a few functional types to represent the phytoplanktonic community, often with a single grouping for diatoms (Séférian et al., 2020; Tréguer et al., 2018). The last generations of ESMs in CMIP6 have improved the representation of phytoplankton ecology by including more functional types (e.g. diazotrophs for some models), which has enhanced model performance. However, diatoms still remain represented by a single group (Séférian et al., 2020). Results from model inter-comparisons highlight the great sensitivity of models to the types of functional groups they include, as well as the ecological traits they represent (Fu et al., 2016; Taucher & Oschlies, 2011). Dutkiewicz et al. (2020) have recently used morphological traits (i.e. cell size), biogeochemical functions and thermal tolerances to define more than 350 phytoplankton types. Their results showed that species richness projections were altered by the number as well as the nature of phytoplankton traits, each controlling a distinct aspect of the species' responses (Dutkiewicz et al., 2020). They concluded that the addition of traits, such as cell shape, might improve model projections (Dutkiewicz et al., 2020). In situ studies have also highlighted the importance of phytoplankton composition for carbon exportation (Dybwad et al., 2021; Henson et al., 2012). However, such models with hundreds of phytoplankton types cannot realistically be used to perform centennial climatic simulations because of computational cost. Hence, although our results with oblates give some support to the ESMs that only considered a single diatom group, they also emphasise that prolates

and dinoflagellates exhibit distinct alterations of their phenology and abundance. Therefore, the distinction of oblate and prolate diatoms as well as dinoflagellates in ESM models may be a simple way to improve model projections because these three groups have different phenologies and responses to climate change, which may affect our current understanding of the consequences of phytoplankton shifts on the biological carbon pump (Karp-Boss & Boss, 2016; Kléparski et al., 2022; Litchman & Klausmeier, 2008; Naselli-Flores et al., 2021; Ryabov et al., 2021).

AUTHOR CONTRIBUTIONS

L.K. and G.B. designed the study, performed the analyses and wrote the first draft. L.K., G.B., M.E. and C.O. discussed the results and reviewed the manuscript.

ACKNOWLEDGMENTS

We acknowledge the World Climate Research Programme, which, through its Working Group on Coupled Modelling, coordinated and promoted CMIP6. We thank the climate modelling groups for producing and making available their model output, the Earth System Grid Federation (ESGF) for archiving the data and providing access, and the multiple funding agencies who support CMIP6 and ESGF. We also thank the owners and crews that have towed the CPRs on a voluntary basis for over 80 years contributing to one of the world's largest and longest ongoing ecological experiments. Without these early pioneers of citizen science and broad-scale volunteer monitoring projects, this unique ecological dataset would never have been financially or logistically viable.

FUNDING INFORMATION

Funding that supports data collection has come from a number of contracts since inception of the Continuous Plankton Recorder survey, the current funded projects include: the UK Natural Environment Research Council, grant/award number: NE/R002738/1 and NE/M007855/1; EMFF; Climate Linked Atlantic Sector Science, grant/award number: NE/ R015953/1, DEFRA UK ME-5308, NSF USA OCE-1657887, DFO CA F5955-150026/001/HAL, NERC UK NC-R8/H12/100, Horizon 2020: 862428 Atlantic Mission and AtlantECO 862923, IMR Norway, DTU Aqua Denmark and the French Ministry of Environment, Energy, and the Sea (MEEM). This work was also financially supported by the European Union, European Regional Development Fund (ERDF), the French State, the French Region Hauts-de-France and Ifremer, in the framework of the project CPER IDEAL 2021–2027. LK also received funds as part of a PhD grant co-financed by the French Region Hauts-de-France region and the Marine Biological Association.

CONFLICT OF INTEREST STATEMENT

The authors declare no conflict of interest.

DATA AVAILABILITY STATEMENT

All the data used in this article are already freely available (see Section 2 and Text S1).

ORCID

Loïck Kléparski https://orcid.org/0000-0002-7536-2941

REFERENCES

Ackerly, D. D. (2003). Community assembly, niche conservatism, and adaptive evolution in changing environments. *International Journal of Plant Sciences*, *164*(S3), S165–S184. https://doi.org/10.1086/368401

Asch, R. G., Stock, C. A., & Sarmiento, J. L. (2019). Climate change impacts on mismatches between phytoplankton blooms and fish spawning phenology. *Global Change Biology*, *25*(8), 2544–2559. https://doi.org/10.1111/gcb.14650

Beaugrand, G. (2015). *Marine biodiversity, climatic variability and global change*. Routledge.

Beaugrand, G., Balembois, A., Kléparski, L., & Kirby, R. R. (2022). Addressing the dichotomy of fishing and climate in fishery management with the FishClim model. *Communications Biology*, *5*(1), 1146. https://doi.org/10.1038/s42003-022-04100-6

Beaugrand, G., Brander, K. M., Lindley, J. A., Souissi, S., & Reid, P. C. (2003). Plankton effect on cod recruitment in the North Sea. *Nature*, *426*(6967), 661–664. https://doi.org/10.1038/nature02164

Beaugrand, G., Conversi, A., Atkinson, A., Cloern, J., Chiba, S., Fonda-Umani, S., Kirby, R. R., Greene, C., Goberville, E., Otto, S. A., Reid, P. C., Stemmann, L., & Edwards, M. (2019). Prediction of unprecedented biological shifts in the global ocean. *Nature Climate Change*, *9*, 10–243.

Beaugrand, G., Edwards, M., Raybaud, V., Goberville, E., & Kirby, R. R. (2015). Future vulnerability of marine biodiversity compared with contemporary and past changes. *Nature Climate Change*, *5*(7), 695–701. https://doi.org/10.1038/nclimate2650

Beaugrand, G., & Kirby, R. R. (2016). Quasi-deterministic responses of marine species to climate change. *Climate Research*, *69*(2), 117–128. https://doi.org/10.3354/cr01398

Beaugrand, G., & Kirby, R. R. (2018). How do Marine pelagic species respond to climate change? Theories and observations. *Annual Review of Marine Science*, *10*(1), 169–197. https://doi.org/10.1146/annurev-marine-121916-063304

Bopp, L., Aumont, O., Cadule, P., Alvain, S., & Gehlen, M. (2005). Response of diatoms distribution to global warming and potential implications: A global model study. *Geophysical Research Letters*, *32*(19), L19606. https://doi.org/10.1029/2005GL023653

Bopp, L., Resplandy, L., Orr, J. C., Doney, S. C., Dunne, J. P., Gehlen, M., Halloran, P., Heinze, C., Ilyina, T., Séférian, R., Tjiputra, J., & Vichi, M. (2013). Multiple stressors of ocean ecosystems in the 21st century: Projections with CMIP5 models. *Biogeosciences*, *10*(10), 6225–6245. https://doi.org/10.5194/bg-10-6225-2013

Boyce, D. G., Petrie, B., Frank, K. T., Worm, B., & Leggett, W. C. (2017). Environmental structuring of marine plankton phenology. *Nature Ecology & Evolution*, *1*(10), 1484–1494. https://doi.org/10.1038/s41559-017-0287-3

Brun, P., Kiørboe, T., Licandro, P., & Payne, M. R. (2016). The predictive skill of species distribution models for plankton in a changing climate. *Global Change Biology*, *22*(9), 3170–3181. https://doi.org/10.1111/gcb.13274

Cabré, A., Shields, D., Marinov, I., & Kostadinov, T. S. (2016). Phenology of size-partitioned phytoplankton carbon-biomass from ocean color remote sensing and CMIP5 models. *Frontiers in Marine Science*, *3*, Article 39, 1–20. https://doi.org/10.3389/fmars.2016.00039

Caracciolo, M., Beaugrand, G., Hélaouët, P., Gevaert, F., Edwards, M., Lizon, F., Kléparski, L., & Goberville, E. (2021). Annual phytoplankton succession results from niche-environment interaction. *Journal of Plankton Research*, *43*(1), 85–102. https://doi.org/10.1093/plankt/fbaa060

Chivers, W. J., Edwards, M., & Hays, G. C. (2020). Phenological shuffling of major marine phytoplankton groups over the last six decades.

Diversity and Distributions, *26*(5), 536–548. https://doi.org/10.1111/ddi.13028

Cushing, D. H. (1990). Plankton production and year-class strength in fish populations: An update of the match/mismatch hypothesis. *Advances in Marine Biology*, *26*, 249–293. https://doi.org/10.1016/S0065-2881(08)60202-3

Dutkiewicz, S., Cermeno, P., Jahn, O., Follows, M. J., Hickman, A. E., Taniguchi, D. A. A., & Ward, B. A. (2020). Dimensions of marine phytoplankton diversity. *Biogeosciences*, *17*(3), 609–634. https://doi.org/10.5194/bg-17-609-2020

Dutkiewicz, S., Scott, J. R., & Follows, M. J. (2013). Winners and losers: Ecological and biogeochemical changes in a warming ocean. *Global Biogeochemical Cycles*, *27*(2), 463–477. https://doi.org/10.1002/gbc.20042

Dybwad, C., Assmy, P., Olsen, L. M., Peeken, I., Nikolopoulos, A., Krumpen, T., Randelhoff, A., Tatarek, A., Wiktor, J. M., & Reigstad, M. (2021). Carbon export in the Seasonal Sea ice zone north of Svalbard from winter to late summer. *Frontiers in Marine Science*, *7*, 525800. https://doi.org/10.3389/fmars.2020.525800

Edwards, M., Beaugrand, G., Kléparski, L., Helaouët, P., & Reid, P. C. (2022). Climate variability and multi-decadal diatom abundance in the Northeast Atlantic. *Communications Earth & Environment*, *3*, 162. https://doi.org/10.1038/s43247-022-00492-9

Edwards, M., Beaugrand, G., Reid, P. C., Rowden, A. A., & Jones, M. B. (2002). Ocean climate anomalies and the ecology of the North Sea. *Marine Ecology Progress Series*, *239*, 1–10. https://doi.org/10.3354/meps239001

Edwards, M., & Richardson, A. J. (2004). Impact of climate change on marine pelagic phenology and trophic mismatch. *Nature*, *430*(7002), 881–884. https://doi.org/10.1038/nature02808

Eyring, V., Bony, S., Meehl, G. A., Senior, C. A., Stevens, B., Stouffer, R. J., & Taylor, K. E. (2016). Overview of the coupled model Intercomparison project phase 6 (CMIP6) experimental design and organization. *Geoscientific Model Development*, *9*(5), 1937–1958. https://doi.org/10.5194/gmd-9-1937-2016

Field, C. B., Behrenfeld, M. J., Randerson, J. T., & Falkowski, P. G. (1998). Primary production of the biosphere: Integrating terrestrial and oceanic components. *Science*, *281*, 237–240.

Friedland, K. D., Mouw, C. B., Asch, R. G., Ferreira, A. S. A., Henson, S. A., Hyde, K. J. W., Morse, R. E., Thomas, A. C., & Brady, D. C. (2018). Phenology and time series trends of the dominant seasonal phytoplankton bloom across global scales. *Global Ecology and Biogeography*, *27*(5), 551–569. https://doi.org/10.1111/geb.12717

Fu, W., Randerson, J. T., & Moore, J. K. (2016). Climate change impacts on net primary production (NPP) and export production (EP) regulated by increasing stratification and phytoplankton communitystructure in the CMIP5 models. *Biogeosciences*, *13*(18), 5151–5170. https://doi.org/10.5194/bg-13-5151-2016

Gause, G. F. (1934). *The struggle for existence*. Williams and Wilkins.

Helaouët, P., & Beaugrand, G. (2007). Macroecology of *Calanus finmarchicus* and *C. helgolandicus* in the North Atlantic Ocean and adjacent seas. *Marine Ecology Progress Series*, *345*, 147–165. https://doi.org/10.3354/meps06775

Henson, S. A., Cole, H., Beaulieu, C., & Yool, A. (2013). The impact of global warming on seasonality of ocean primary production. *Biogeosciences*, *10*, 4357–4369. https://doi.org/10.5194/bg-10-4357-2013

Henson, S. A., Cole, H. S., Hopkins, J., Martin, A. P., & Yool, A. (2018). Detection of climate change-driven trends in phytoplankton phenology. *Global Change Biology*, *24*, e101–e111. https://doi.org/10.1111/gcb.13886

Henson, S. A., Lampitt, R., & Johns, D. (2012). Variability in phytoplankton community structure in response to the North Atlantic oscillation and implications for organic carbon flux. *Limnology and Oceanography*, *57*(6), 1591–1601. https://doi.org/10.4319/lo.2012.57.6.1591

Henson, S. A., Laufkötter, C., Leung, S., Giering, S. L. C., Palevsky, H. I., & Cavan, E. L. (2022). Uncertain response of ocean biological carbon export in a changing world. *Nature Geoscience*, *15*(4), 248–254. https://doi.org/10.1038/s41561-022-00927-0

Hutchinson, G. E. (1957). Concluding remarks. *Cold Spring Harbor Symposia on Quantitative Biology*, *22*, 415–427.

Hutchinson, G. E. (1978). *An introduction to population ecology*. Yale University Press.

IPCC. (2019). Technical summary. In D. C. Roberts, H. O. Pörtner, V. Masson-Delmotte, P. Zhai, E. Poloczanska, K. Mintenbeck, M. Tignor, A. Alegria, M. Nicolai, A. Okem, J. Petzold, B. Rama, & N. M. Weyer (Eds.), *IPCC special report on the ocean and cryosphere in a changing climate* (pp. 39–69). Cambridge University Press.

Irwin, A. J., Nelles, A. M., & Finkel, Z. V. (2012). Phytoplankton niches estimated from field data. *Limnology and Oceanography*, *57*(3), 787–797. https://doi.org/10.4319/lo.2012.57.3.0787

Jonas, T. D., Walne, A. W., Beaugrand, G., Gregory, L., & Hays, G. C. (2004). The volume of water filtered by a continuous plankton recorder sample: The effect of ship speed. *Journal of Plankton Research*, *26*(12), 1499–1506. https://doi.org/10.1093/plankt/fbh137

Karp-Boss, L., & Boss, E. (2016). The elongated, the squat and the spherical: Selective pressures for phytoplankton shape. In P. M. Glibert & T. M. Kana (Eds.), *Aquatic microbial ecology and biogeochemistry: A dual perspective* (pp. 25–34). Springer International Publishing. https://doi.org/10.1007/978-3-319-30259-1_3

Kemp, A. E. S., & Villareal, T. A. (2013). High diatom production and export in stratified waters – A potential negative feedback to global warming. *Progress in Oceanography*, *119*, 4–23. https://doi.org/10.1016/j.pocean.2013.06.004

Kemp, A. E. S., & Villareal, T. A. (2018). The case of the diatoms and the muddled mandalas: Time to recognize diatom adaptations to stratified waters. *Progress in Oceanography*, *167*, 138–149. https://doi.org/10.1016/j.pocean.2018.08.002

Kléparski, L., Beaugrand, G., Edwards, M., Schmitt, F. G., Kirby, R. R., Breton, E., Gevaert, F., & Maniez, E. (2022). Morphological traits, niche-environment interaction and temporal changes in diatoms. *Progress in Oceanography*, *201*, 102747. https://doi.org/10.1016/j.pocean.2022.102747

Kwiatkowski, L., Torres, O., Bopp, L., Aumont, O., Chamberlain, M., Christian, J. R., Dunne, J. P., Gehlen, M., Ilyina, T., John, J. G., Lenton, A., Li, H., Lovenduski, N. S., Orr, J. C., Palmieri, J., Santana-Falcón, Y., Schwinger, J., Séférian, R., Stock, C. A., … Ziehn, T. (2020). Twenty-first century ocean warming, acidification, deoxygenation, and upper-ocean nutrient and primary production decline from CMIP6 model projections. *Biogeosciences*, *17*(13), 3439–3470. https://doi.org/10.5194/bg-17-3439-2020

Lewandowska, A., & Sommer, U. (2010). Climate change and the spring bloom: A mesocosm study on the influence of light and temperature on phytoplankton and mesozooplankton. *Marine Ecology Progress Series*, *405*, 101–111. https://doi.org/10.3354/meps08520

Litchman, E., Edwards, K. F., Klausmeier, C. A., & Thomas, M. K. (2012). Phytoplankton niches, traits and eco-evolutionary responses to global environmental change. *Marine Ecology Progress Series*, *470*, 235–248. https://doi.org/10.3354/meps09912

Litchman, E., & Klausmeier, C. A. (2008). Trait-based community ecology of phytoplankton. *Annual Review of Ecology, Evolution, and Systematics*, *39*(1), 615–639.

Litchman, E., Klausmeier, C. A., Schofield, O. M., & Falkowski, P. G. (2007). The role of functional traits and trade-offs in structuring phytoplankton communities: Scaling from cellular to ecosystem level. *Ecology Letters*, *10*(12), 1170–1181. https://doi.org/10.1111/j.1461-0248.2007.01117.x

Lürling, M. (2021). Grazing resistance in phytoplankton. *Hydrobiologia*, *848*(1), 237–249. https://doi.org/10.1007/s10750-020-04370-3

Mannocci, L., Boustany, A. M., Roberts, J. J., Palacios, D. M., Dunn, D. C., Halpin, P. N., Viehman, S., Moxley, J., Cleary, J., Bailey, H., Bograd, S. J., Becker, E. A., Gardner, B., Hartog, J. R., Hazen, E. L., Ferguson, M. C., Forney, K. A., Kinlan, B. P., Oliver, M. J., … Winship,

A. J. (2017). Temporal resolutions in species distribution models of highly mobile marine animals: Recommendations for ecologists and managers. *Diversity and Distributions*, *23*(10), 1098–1109. https://doi.org/10.1111/ddi.12609

Margalef, R. (1978). Life-forms of phytoplankton as survival alternatives in an unstable environment. *Oceanologica Acta*, *1*(4), 493–509.

Marinov, I., Doney, S. C., & Lima, I. D. (2010). Response of ocean phytoplankton community structure to climate change over the 21st century: Partitioning the effects of nutrients, temperature and light. *Biogeosciences*, *7*, 3941–3959. https://doi.org/10.5194/bg-7-3941-2010

Martin, T. L., & Huey, R. B. (2008). Why "suboptimal" is optimal: Jensen's inequality and ectotherm thermal preferences. *The American Naturalist*, *171*(3), E102–E118. https://doi.org/10.1086/527502

Miller, C. B. (2004). *Biological oceanography*. Blackwell Science Ltd.

Naselli-Flores, L., Zohary, T., & Padisák, J. (2021). Life in suspension and its impact on phytoplankton morphology: An homage to Colin S. Reynolds. *Hydrobiologia*, *848*, 7–30. https://doi.org/10.1007/s10750-020-04217-x

O'Neill, B. C., Kriegler, E., Ebi, K. L., Kemp-Benedict, E., Riahi, K., Rothman, D. S., van Ruijven, B. J., van Vuuren, D. P., Birkmann, J., Kok, K., Levy, M., & Solecki, W. (2017). The roads ahead: Narratives for shared socioeconomic pathways describing world futures in the 21st century. *Global Environmental Change*, *42*, 169–180. https://doi.org/10.1016/j.gloenvcha.2015.01.004

O'Neill, B. C., Tebaldi, C., van Vuuren, D. P., Eyring, V., Friedlingstein, P., Hurtt, G., Knutti, R., Kriegler, E., Lamarque, J., Lowe, J., Meehl, G. A., Moss, R., Riahi, K., & Sanderson, B. M. (2016). The scenario model Intercomparison project (ScenarioMIP) for CMIP6. *Geoscientific Model Development*, *9*(9), 3461–3482. https://doi.org/10.5194/gmd-9-3461-2016

Padisak, J., Soroczki-Pinter, E., & Rezner, Z. (2003). Sinking properties of some phytoplankton shapes and the relation of form resistance to morphological diversity of plankton—An experimental study. *Hydrobiologia*, *500*, 243–257.

Pančić, M., & Kiørboe, T. (2018). Phytoplankton defence mechanisms: Traits and trade-offs: Defensive traits and trade-offs. *Biological Reviews*, *93*(2), 1269–1303. https://doi.org/10.1111/brv.12395

Passow, U., & Carlson, C. A. (2012). The biological pump in a high CO_2 world. *Marine Ecology Progress Series*, *470*, 249–271. https://doi.org/10.3354/meps09985

Poloczanska, E. S., Brown, C. J., Sydeman, W. J., Kiessling, W., Schoeman, D. S., Moore, P. J., Brander, K., Bruno, J. F., Buckley, L. B., Burrows, M. T., Duarte, C. M., Halpern, B. S., Holding, J., Kappel, C. V., O'Connor, M. I., Pandolfi, J. M., Parmesan, C., Schwing, F., Thompson, S. A., & Richardson, A. J. (2013). Global imprint of climate change on marine life. *Nature Climate Change*, *3*(10), 919–925. https://doi.org/10.1038/nclimate1958

Pulliam, H. R. (2000). On the relationship between niche and distribution. *Ecology Letters*, *3*(4), 349–361. https://doi.org/10.1046/j.1461-0248.2000.00143.x

Raven, J. A., & Waite, A. M. (2004). The evolution of silicification in diatoms: Inescapable sinking and sinking as escape? *New Phytologist*, *162*(1), 45–61. https://doi.org/10.1111/j.1469-8137.2004.01022.x

Reid, P. C., Colebrook, J. M., Matthews, J. B. L., Aiken, J., & Continuous Plankton Recorder Team. (2003). The continuous plankton recorder: Concepts and history, from plankton indicator to undulating recorders. *Progress in Oceanography*, *58*(2–4), 117–173. https://doi.org/10.1016/j.pocean.2003.08.002

Richardson, A. J., Walne, A. W., John, A. W. G., Jonas, T. D., Lindley, J. A., Sims, D. W., Stevens, D., & Witt, M. (2006). Using continuous plankton recorder data. *Progress in Oceanography*, *68*(1), 27–74. https://doi.org/10.1016/j.pocean.2005.09.011

Ryabov, A., Kerimoglu, O., Litchman, E., Olenina, I., Roselli, L., Basset, A., Stanca, E., & Blasius, B. (2021). Shape matters: The relationship between cell geometry and diversity in phytoplankton. *Ecology Letters*, *24*(4), 847–861. https://doi.org/10.1111/ele.13680

Séférian, R., Berthet, S., Yool, A., Palmiéri, J., Bopp, L., Tagliabue, A., Kwiatkowski, L., Aumont, O., Christian, J., Dunne, J., Gehlen, M., Ilyina, T., John, J. G., Li, H., Long, M. C., Luo, J. Y., Nakano, H., Romanou, A., Schwinger, J., … Yamamoto, A. (2020). Tracking improvement in simulated marine biogeochemistry between CMIP5 and CMIP6. *Current Climate Change Reports*, *6*(3), 95–119. https://doi.org/10.1007/s40641-020-00160-0

Smayda, T. (1970). The suspension and sinking of phytoplankton in the sea. *Oceanography and Marine Biology*, *8*, 353–414.

Smetacek, V. (1985). Role of sinking in diatom life-history cycles: Ecological, evolutionary and geological significance. *Marine Biology*, *84*, 239–251.

Soberon, J., & Nakamura, M. (2009). Niches and distributional areas: Concepts, methods, and assumptions. *Proceedings of the National Academy of Sciences of the United States of America*, *106*(Suppl._2), 19644–19650. https://doi.org/10.1073/pnas.0901637106

Sournia, A. (1982). Form and function in marine phytoplankton. *Biological Reviews*, *57*, 347–394.

Stock, C. A., Alexander, M. A., Bond, N. A., Brander, K. M., Cheung, W. W. L., Curchitser, E. N., Delworth, T. L., Dunne, J. P., Griffies, S. M., Haltuch, M. A., Hare, J. A., Hollowed, A. B., Lehodey, P., Levin, S. A., Link, J. S., Rose, K. A., Rykaczewski, R. R., Sarmiento, J. L., Stouffer, R., … Werner, F. E. (2011). On the use of IPCC-class models to assess the impact of climate on living marine resources. *Progress in Oceanography*, *88*, 1–27. https://doi.org/10.1016/j.pocean.2010.09.001

Straile, D., Kerimoglu, O., & Peeters, F. (2015). Trophic mismatch requires seasonal heterogeneity of warming. *Ecology*, *96*(10), 2794–2805. https://doi.org/10.1890/14-0839.1

Taucher, J., & Oschlies, A. (2011). Can we predict the direction of marine primary production change under global warming? *Geophysical Research Letters*, *38*, L02603. https://doi.org/10.1029/2010GL045934

Thackeray, S. J., Henrys, P. A., Hemming, D., Bell, J. R., Botham, M. S., Burthe, S., Helaouet, P., Johns, D. G., Jones, I. D., Leech, D. I., Mackay, E. B., Massimino, D., Atkinson, S., Bacon, P. J., Brereton, T. M., Carvalho, L., Clutton-Brock, T. H., Duck, C., Edwards, M., … Wanless, S. (2016). Phenological sensitivity to climate across taxa and trophic levels. *Nature*, *535*(7611), 241–245. https://doi.org/10.1038/nature18608

Thomas, M. K., Kremer, C. T., Klausmeier, C. A., & Litchman, E. (2012). A global pattern of thermal adaptation in marine phytoplankton. *Science*, *338*(6110), 1085–1088. https://doi.org/10.1126/science.1224836

Tréguer, P., Bowler, C., Moriceau, B., Dutkiewicz, S., Gehlen, M., Aumont, O., Bittner, L., Dugdale, R., Finkel, Z., Iudicone, D., Jahn, O., Guidi, L., Lasbleiz, M., Leblanc, K., Levy, M., & Pondaven, P. (2018). Influence of diatom diversity on the ocean biological carbon pump. *Nature Geoscience*, *11*(1), 27–37. https://doi.org/10.1038/s41561-017-0028-x

van der Spoel, S. (1994). The basis for boundaries in pelagic biogeography. *Progress in Oceanography*, *34*(2–3), 121–133. https://doi.org/10.1016/0079-6611(94)90005-1

Ward, B. A., & Follows, M. J. (2016). Marine mixotrophy increases trophic transfer efficiency, mean organism size, and vertical carbon flux. *Proceedings of the National Academy of Sciences of the United States of America*, *113*(11), 2958–2963. https://doi.org/10.1073/pnas.1517118113

Warner, A. J., & Hays, G. C. (1994). Sampling by the continuous plankton recorder survey. *Progress in Oceanography*, *34*(2–3), 237–256. https://doi.org/10.1016/0079-6611(94)90011-6

Winder, M., & Schindler, D. E. (2004). Climate change uncouples trophic interactions in an aquatic ecosystem. *Ecology*, *85*(8), 2100–2106. https://doi.org/10.1890/04-0151

Yamaguchi, R., Rodgers, K. B., Stein, K. J., Timmermann, A., Schlunegger, S., Bianchi, D., Dunne, J. P., & Slater, R. D. (2022). Trophic level

decoupling drives future change in phytoplankton bloom phenology. *Nature Climate Change*, *12*, 469–476. https://doi.org/10.1038/s41558-022-01353-1

DATA SOURCES

Boucher, O., Denvil, S., Levavasseur, G., Cozic, A., Caubel, A., Foujols, M.-A., Meurdesoif, Y., Cadule, P., Devilliers, M., Ghattas, J., Lebas, N., Lurton, T., Mellul, L., Musat, I., Mignot, J., & Cheruy, F. (2018). *IPSL IPSL-CM6A-LR model output prepared for CMIP6 CMIP historical. Version 2018-07-31*. Earth System Grid Federation. https://doi.org/10.22033/ESGF/CMIP6.5195

Boucher, O., Denvil, S., Levavasseur, G., Cozic, A., Caubel, A., Foujols, M.-A., Meurdesoif, Y., Cadule, P., Devilliers, M., Dupont, E., & Lurton, T. (2019). *IPSL IPSL-CM6A-LR model output prepared for CMIP6 ScenarioMIP ssp126. Version 2019-08-05*. Earth System Grid Federation. https://doi.org/10.22033/ESGF/CMIP6.5262

Boucher, O., Denvil, S., Levavasseur, G., Cozic, A., Caubel, A., Foujols, M.-A., Meurdesoif, Y., Cadule, P., Devilliers, M., Dupont, E., & Lurton, T. (2019). *IPSL IPSL-CM6A-LR model output prepared for CMIP6 ScenarioMIP ssp245. Version 2019-07-30*. Earth System Grid Federation. https://doi.org/10.22033/ESGF/CMIP6.5264

Boucher, O., Denvil, S., Levavasseur, G., Cozic, A., Caubel, A., Foujols, M.-A., Meurdesoif, Y., Cadule, P., Devilliers, M., Dupont, E., & Lurton, T. (2019). *IPSL IPSL-CM6A-LR model output prepared for CMIP6 ScenarioMIP ssp585. Version 2019-08-22*. Earth System Grid Federation. https://doi.org/10.22033/ESGF/CMIP6.5271

Good, P., Sellar, A., Tang, Y., Rumbold, S., Ellis, R., Kelley, D., & Kuhlbrodt, T. (2019). *MOHC UKESM1.0-LL model output prepared for CMIP6 ScenarioMIP ssp126. Version 2019-07-04*. Earth System Grid Federation. https://doi.org/10.22033/ESGF/CMIP6.6333

Good, P., Sellar, A., Tang, Y., Rumbold, S., Ellis, R., Kelley, D., & Kuhlbrodt, T. (2019). *MOHC UKESM1.0-LL model output prepared for CMIP6 ScenarioMIP ssp245. Version 2019-07-08*. Earth System Grid Federation. https://doi.org/10.22033/ESGF/CMIP6.6339

Good, P., Sellar, A., Tang, Y., Rumbold, S., Ellis, R., Kelley, D., & Kuhlbrodt, T. (2019). *MOHC UKESM1.0-LL model output prepared for CMIP6 ScenarioMIP ssp585. Version 2019-07-24*. Earth System Grid Federation. https://doi.org/10.22033/ESGF/CMIP6.6405

John, J. G., Blanton, C., McHugh, C., Radhakrishnan, A., Rand, K., Vahlenkamp, H., Wilson, C., Zadeh, N. T., Dunne, J. P., Dussin, R., Horowitz, L. W., Krasting, J. P., Lin, P., Malyshev, S., Naik, V., Ploshay, J., Shevliakova, E., Silvers, L., Stock, C., … Zeng, Y. (2018). *NOAA-GFDL GFDL-ESM4 model output prepared for CMIP6 ScenarioMIP ssp126. Version 2019-06-19*. Earth System Grid Federation. https://doi.org/10.22033/ESGF/CMIP6.8684

John, J. G., Blanton, C., McHugh, C., Radhakrishnan, A., Rand, K., Vahlenkamp, H., Wilson, C., Zadeh, N. T., Dunne, J. P., Dussin, R., Horowitz, L. W., Krasting, J. P., Lin, P., Malyshev, S., Naik, V., Ploshay, J., Shevliakova, E., Silvers, L., Stock, C., … Zeng, Y. (2018). *NOAA-GFDL GFDL-ESM4 model output prepared for CMIP6 ScenarioMIP ssp245. Version 2019-06-18*. Earth System Grid Federation. https://doi.org/10.22033/ESGF/CMIP6.8686

John, J. G., Blanton, C., McHugh, C., Radhakrishnan, A., Rand, K., Vahlenkamp, H., Wilson, C., Zadeh, N. T., Dunne, J. P., Dussin, R., Horowitz, L. W., Krasting, J. P., Lin, P., Malyshev, S., Naik, V., Ploshay, J., Shevliakova, E., Silvers, L., Stock, C., … Zeng, Y. (2018). *NOAA-GFDL GFDL-ESM4 model output prepared for CMIP6 ScenarioMIP ssp585. Version 2019-06-19*. Earth System Grid Federation. https://doi.org/10.22033/ESGF/CMIP6.8706

Krasting, J. P., John, J. G., Blanton, C., McHugh, C., Nikonov, S., Radhakrishnan, A., Rand, K., Zadeh, N. T., Balaji, V., Durachta, J., Dupuis, C., Menzel, R., Robinson, T., Underwood, S., Vahlenkamp, H., Dunne, K. A., Gauthier, P. P. G., Ginoux, P., Griffies, S. M., … Zhao, M. (2018). *NOAA-GFDL GFDL-ESM4 model output prepared for CMIP6 CMIP historical. Version 2019-08-03*. Earth System Grid Federation. https://doi.org/10.22033/ESGF/CMIP6.8597

Seferian, R. (2018). *CNRM-CERFACS CNRM-ESM2-1 model output prepared for CMIP6 CMIP historical. Version 2018-10-23*. Earth System Grid Federation. https://doi.org/10.22033/ESGF/CMIP6.4068

Seland, Ø., Bentsen, M., Oliviè, D. J. L., Toniazzo, T., Gjermundsen, A., Graff, L. S., Debernard, J. B., Gupta, A. K., He, Y., Kirkevåg, A., Schwinger, J., Tjiputra, J., Aas, K. S., Bethke, I., Fan, Y., Griesfeller, J., Grini, A., Guo, C., Ilicak, M., … Schulz, M. (2019). *NCC NorESM2-LM model output prepared for CMIP6 CMIP historical. Version 2019-08-16*. Earth System Grid Federation. https://doi.org/10.22033/ESGF/CMIP6.8036

Seland, Ø., Bentsen, M., Oliviè, D. J. L., Toniazzo, T., Gjermundsen, A., Graff, L. S., Debernard, J. B., Gupta, A. K., He, Y., Kirkevåg, A., Schwinger, J., Tjiputra, J., Aas, K. S., Bethke, I., Fan, Y., Griesfeller, J., Grini, A., Guo, C., Ilicak, M., … Schulz, M. (2019). *NCC NorESM2-LM model output prepared for CMIP6 ScenarioMIP ssp126. Version 2019-12-19*. Earth System Grid Federation. https://doi.org/10.22033/ESGF/CMIP6.8248

Seland, Ø., Bentsen, M., Oliviè, D. J. L., Toniazzo, T., Gjermundsen, A., Graff, L. S., Debernard, J. B., Gupta, A. K., He, Y., Kirkevåg, A., Schwinger, J., Tjiputra, J., Aas, K. S., Bethke, I., Fan, Y., Griesfeller, J., Grini, A. G., Chuncheng, I., Ilicak, M., … Schulz, M. (2019). *NCC NorESM2-LM model output prepared for CMIP6 ScenarioMIP ssp245. Version 2019-12-30*. Earth System Grid Federation. https://doi.org/10.22033/ESGF/CMIP6.8253

Seland, Ø., Bentsen, M., Oliviè, D. J. L., Toniazzo, T., Gjermundsen, A., Graff, L. S., Debernard, J. B., Gupta, A. K., He, Y., Kirkevåg, A., Schwinger, J., Tjiputra, J., Aas, K. S., Bethke, I., Fan, Y., Griesfeller, J., Grini, A., Guo, C., Ilicak, M., … Schulz, M. (2019). *NCC NorESM2-LM model output prepared for CMIP6 ScenarioMIP ssp585. Version 2019-12-21*. Earth System Grid Federation. https://doi.org/10.22033/ESGF/CMIP6.8319

Tang, Y., Rumbold, S., Ellis, R., Kelley, D., Mulcahy, J., Sellar, A., Walton, J., & Jones, C. (2019). *MOHC UKESM1.0-LL model output prepared for CMIP6 CMIP historical. Version 2019-06-25*. Earth System Grid Federation. https://doi.org/10.22033/ESGF/CMIP6.6113

Voldoire, A. (2019). *CNRM-CERFACS CNRM-ESM2-1 model output prepared for CMIP6 ScenarioMIP ssp126. Version 2018-11-12*. Earth System Grid Federation. https://doi.org/10.22033/ESGF/CMIP6.4186

Voldoire, A. (2019). *CNRM-CERFACS CNRM-ESM2-1 model output prepared for CMIP6 ScenarioMIP ssp245. Version 2018-10-26*. Earth System Grid Federation. https://doi.org/10.22033/ESGF/CMIP6.4191

Voldoire, A. (2019). *CNRM-CERFACS CNRM-ESM2-1 model output prepared for CMIP6 ScenarioMIP ssp585. Version 2019-10-11*. Earth System Grid Federation. https://doi.org/10.22033/ESGF/CMIP6.4226

Wieners, K.-H., Giorgetta, M., Jungclaus, J., Reick, C., Esch, M., Bittner, M., Legutke, S., Schupfner, M., Wachsmann, F., Gayler, V., Haak, H., de Vrese, P., Raddatz, T., Mauritsen, T., von Storch, J.-S., Behrens, J., Brovkin, V., Claussen, M., Crueger, T., … Roeckner, E. (2019). *MPI-M MPI-ESM1.2-LR model output prepared for CMIP6 CMIP historical. Version 2019-09-11*. Earth System Grid Federation. https://doi.org/10.22033/ESGF/CMIP6.6595

Wieners, K.-H., Giorgetta, M., Jungclaus, J., Reick, C., Esch, M., Bittner, M., Gayler, V., Haak, H., de Vrese, P., Raddatz, T., Mauritsen, T., von Storch, J.-S., Behrens, J., Brovkin, V., Claussen, M., Crueger, T., Fast, I., Fiedler, S., Hagemann, S., … Roeckner, E. (2019). *MPI-M MPI-ESM1.2-LR model output prepared for CMIP6 ScenarioMIP ssp126. Version 2019-10-29*. Earth System Grid Federation. doi:10.22033/ESGF/CMIP6.6690

Wieners, K.-H., Giorgetta, M., Jungclaus, J., Reick, C., Esch, M., Bittner, M., Gayler, V., Haak, H., de Vrese, P., Raddatz, T., Mauritsen, T., von Storch, J.-S., Behrens, J., Brovkin, V., Claussen, M., Crueger, T., Fast, I., Fiedler, S., Hagemann, S., … Roeckner, E. (2019). *MPI-M MPI-ESM1.2-LR model output prepared for CMIP6 ScenarioMIP ssp245. Version 2019-11-05*. Earth System Grid Federation. https://doi.org/10.22033/ESGF/CMIP6.6693

Wieners, K.-H., Giorgetta, M., Jungclaus, J., Reick, C., Esch, M., Bittner, M., Gayler, V., Haak, H., de Vrese, P., Raddatz, T., Mauritsen, T., von Storch, J.-S., Behrens, J., Brovkin, V., Claussen, M., Crueger, T., Fast, I., Fiedler, S., Hagemann, S., … Roeckner, E. (2019). *MPI-M MPI-ESM1.2-LR model output prepared for CMIP6 ScenarioMIP ssp585. Version 2019-11-12*. Earth System Grid Federation. https://doi.org/10.22033/ESGF/CMIP6.6705

CPR DATA

Helaouët, P. (2021). Marine Biological Association of the UK (MBA) (2021): Continuous Plankton Recorder data. The Archive for Marine Species and Habitats Data (DASSH). https://doi.org/10.17031/1708

ERA5 DATA

Hersbach, H., Bell, B., Berrisford, P., Biavati, G., Horányi, A., Muñoz Sabater, J., Nicolas, J., Peubey, C., Radu, R., Rozum, I., Schepers, D., Simmons, A., Soci, C., Dee, D., & Thépaut, J.-N. (2023). ERA5 hourly data on pressure levels from 1940 to present. Copernicus Climate Change Service (C3S) Climate Data Store (CDS). Retrieved 2 December 2022, from https://doi.org/10.24381/cds.bd0915c6

Copernicus Climate Change Service, Climate Data Store. (2023). ERA5 hourly data on pressure levels from 1940 to present. Copernicus Climate Change Service (C3S) Climate Data Store (CDS). Retrieved 2 December 2022, from https://doi.org/10.24381/cds.bd0915c6

WORLD OCEAN ATLAS 2018

Boyer, T. P., Garcia, H. E., Locarnini, R. A., Zweng, M. M., Mishonov, A. V., Reagan, J. R., Weathers, K. A., Baranova, O. K., Seidov, D., and Smolyar, I. V. (2018). World Ocean Atlas 2018. Dissolved Inorganic Nutrients (phosphate, nitrate and nitrate+nitrite, silicate). NOAA National Centers for Environmental Information. Dataset. Retrieved 6 December 2022, from https://www.ncei.noaa.gov/archive/accession/NCEI-WOA18

SUPPORTING DATA

Kléparski, L., Beaugrand, G., Edwards, M., & Ostle, C. (2023). Phytoplankton life strategies, phenological shifts and climate change in the North Atlantic Ocean from 1850-2100, Dryad, Dataset. https://doi.org/10.5061/dryad.nzs7h44wh

SUPPORTING INFORMATION

Additional supporting information can be found online in the Supporting Information section at the end of this article.

How to cite this article: Kléparski, L., Beaugrand, G., Edwards, M., & Ostle, C. (2023). Phytoplankton life strategies, phenological shifts and climate change in the North Atlantic Ocean from 1850 to 2100. *Global Change Biology*, *29*, 3833–3849. https://doi.org/10.1111/gcb.16709